NORTHWESTERN UNIVERSITY

Quantitative Myocardial Perfusion

A DISSERTATION

SUBMITTED TO THE GRADUATE SCHOOL

IN PARTIAL FULFILLMENT OF THE REUIQREMENT

for the degree

DOCTOR OF PHILOSOPHY

Field of Biomedical Engineering

By

Neil Chatterjee

EVANSTON, ILLINOIS

December 2016

Abstract

Myocardial perfusion is an important marker of cardiovascular health that is routinely evaluated clinically. Perfusion is measured most often using single photon emission computed tomography (SPECT) imaging, but magnetic resonance imaging (MRI) has many advantages over SPECT. Measuring perfusion quantitatively in ml/min/g would theoretically allow for improved characterization of cardiac disease, especially in cases where there is a global perfusion deficit or where perfusion is tracked longitudinally over time. However, there are currently no widely available ways of measuring myocardial perfusion quantitatively in ml/min/g using MRI. Some methods, such as dual bolus and dual echo imaging, have been proposed but none have gained widespread adoption. Described here is a new method for improving the accuracy and ease of use of these existing techniques. Additionally, the measurement of myocardial blood volume is described, which is a separate biomarker that is related to myocardial perfusion and whose measurement is a critical first step in implementing a new method for measuring myocardial perfusion.

Acknowledgements

I'd like to thank my advisor and mentor Tim Carroll for taking me into his lab and providing so much guidance along the way. I'd also like to thank the other current and former students in our lab, especially Parmede Vakil and Charles Cantrell, who were always there to bounce ideas off of and help out. Without Daniel Lee and Brandon Benefield, I wouldn't have had the amazing datasets that made this work possible. Lastly, to my friends and family, I can still hardly believe you put up with me during grad school, and your support has been invaluable.

Dedicated to my loving parents, Arun and Cynthia, and our dog (my “little brother”) Eddie

Table of Contents

List of Tables and Figures

Chapter 1: Background

1.1: Introduction

Myocardial perfusion, the amount of local tissue blood flow in heart muscle, plays a critical role in the diagnosis of coronary artery disease, guiding decisions regarding revascularization, and predicting a patient's future risk of a cardiac event. In addition to its role in coronary artery disease, abnormalities in myocardial perfusion have also been identified in other diseases such as cardiomyopathy[1], coarctation of the aorta[2], and certain cardiovascular risk factors[3] .

The clinical measurement of myocardial perfusion has long been dominated by nuclear imaging -principally single photon emission computed tomography (SPECT)[4]. More recently, MRI has emerged as an alternative way to measure cardiac perfusion. MRI has significant advantages over SPECT including much higher resolution (**Figure 1**), no required radiation dose, and the potential for quantitative measurement of perfusion in ml/min/g. MRI measurement of myocardial perfusion has been the subject of much research and has been described in a number of review articles [5-9]. The most common way to measure perfusion with cardiac magnetic resonance (CMR) is via the "first pass" technique. A bolus of contrast is injected in a peripheral vein, contrast enhancement is observed as the bolus passes through the myocardium, and mathematical analysis of the shape of the time-signal intensity curve measured in the myocardium is used to quantify the tissue perfusion. There are other techniques for measuring perfusion with MRI, but they have notable drawbacks. Arterial spin labeling (ASL) [10] is a promising technique that uses no exogenous contrast, but has less contrast to noise ratio (CNR) than traditional first pass methods. Blood Oxygen Level Dependent (BOLD) imaging [11] also

uses no exogenous contrast, but its interpretation for quantitative perfusion can be complicated because it also depends on factors such as oxygen extraction fraction. Not surprisingly, the overwhelming majority of cardiac perfusion scans, including most if not all clinical scans, use a first pass contrast bolus. The overarching aim of the work presented in this dissertation is to improve the methodology for quantitative myocardial perfusion in a way that makes it conducive for translation to real clinical environments. As such, the body of work in this dissertation concerns only first pass contrast perfusion.

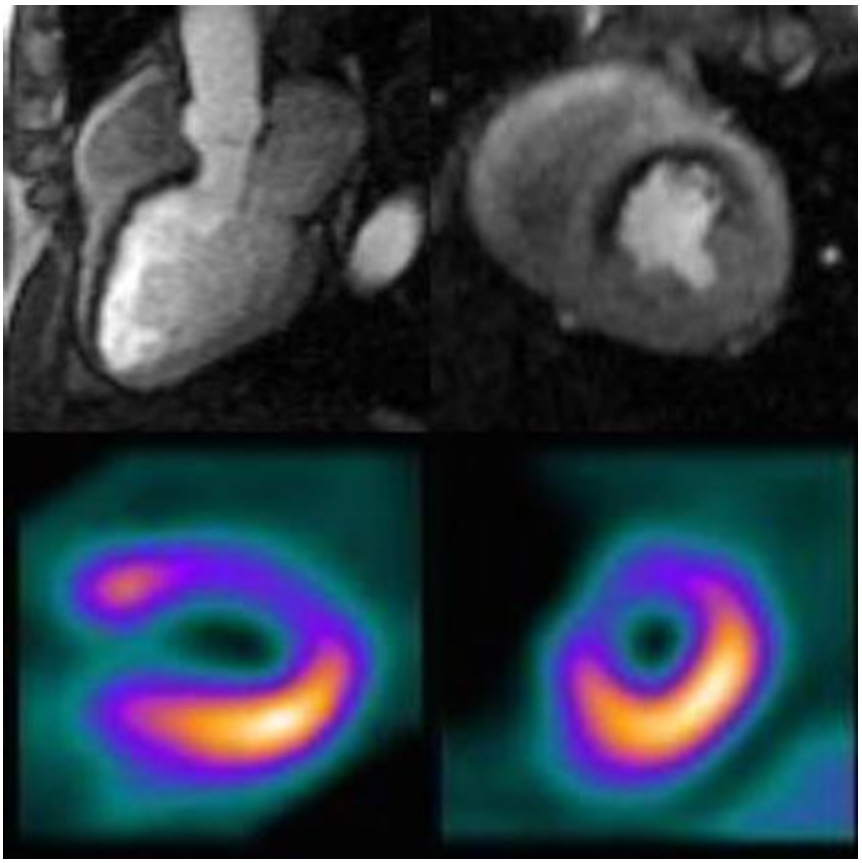

Figure 1: MRI vs SPECT perfusion images
Severe ischemia in the distribution of the left anterior descending coronary artery seen by MR perfusion (top row) and SPECT imaging (bottom row). A single frame from the first-pass MR perfusion series demonstrates severe ischemia of the anteroseptum from base to apex in the 3-chamber view (top left) and of the septal and anterior walls in the mid-chamber short axis view (top right). On SPECT imaging, a similar distribution of ischemia is seen on the vertical long axis (bottom left) and mid-chamber short axis view (bottom right).

1.2: Image Acquisition

The first step in any cardiac perfusion scan is the choice of a pulse sequence to acquire the data. Unfortunately, there is no consensus best sequence, and each type has its own strengths and drawbacks. This section provides a brief overview of the major sequence types currently used

and relevant parameters that are important to data quality. Some text and figures in this chapter are reprinted with permission from [12].

1.2.1 Constraints & Requirements

The choice of which pulse sequence to use is a key determinant of image contrast, spatial & temporal resolution, coverage, and degree of artifacts. These characteristics are usually at odds with one another -- for example gains in contrast may come at the expense resolution or coverage -- and selecting the right sequence requires weighing these competing gains and losses against each other. Consequently, when selecting a perfusion sequence, it is critical to consider the basic requirements for cardiac perfusion imaging. These are:

1) **Strong T1 contrast.** The contrast agent used in MRI perfusion significantly alters the T1 of the myocardium during first pass, therefore T1 sensitive image contrast is desirable.
2) **Coverage of relevant myocardium**. Usually this includes at minimum one short axis slice each through the base, middle, and apex of the myocardium
3) **Spatial Resolution**. At minimum, most sequences must be able to distinguish between subendocardial and transmural ischemia
4) **Temporal Resolution**. To adequately sample flow at the myocardial level, images must be acquired every 1-2 heartbeats. For quantitative perfusion, there is the additional requirement of being able to adequately sample the input function within the blood pool of the left ventricle (LV). Because contrast passes much quicker through the LV than the myocardium, this usually requires sampling every heartbeat.

5) **Lack of Artifacts.** In particular, the dark rim artifact is a specific property of MRI perfusion images that can mimic perfusion defects resulting in potential for misinterpretation and should be minimized.

In meeting these requirements, perfusion imaging has a critical constraint that is absent in much of CMR: because characterizing the bolus passage requires acquiring a full image every 1-2 heart beats, segmented acquisition (as is used in Cine and Late Gadolinium Enhanced imaging) is limited or impossible. In order to achieve full heart coverage, typically three short axis images must be acquired within the time course of a single heartbeat. This limits perfusion imaging to very time-efficient pulse sequences that reduce the time to acquire an image to ~100 ms. The image acquisition time is determined by the length of the cardiac cycle which is often shortened by vasodilator stress.

1.2.2 Preparation Pulses

At the most basic level, a T_1 weighted image is acquired by perturbing the longitudinal magnetization (M_Z) away from equilibrium through the application of an RF pulse at the beginning of the pulse sequence and then acquiring images before the magnetization has a chance to return to normal. As a general rule, blood, fat, and myocardium with short T_1 will return to its unperturbed state faster, appearing bright in a T1-weighted images. There are two approaches to perturb M_Z in cardiac perfusion imaging: with a 180 degree (i.e. an inversion) RF pulse in inversion recovery (IR) exams and a 90 degree RF pulse which completely eliminates or "saturates" MRI signal in a so-called saturation recovery (SR) exams. The SR and IR pulses are often referred to as magnetization preparation pulses and are separate from the RF pulses played

during the image acquisition or image "readout", both of which must be considered in the optimization of a cardiac perfusion exam.

Historically, IR was used for CMR perfusion. Because IR is a 180 degree pulse, it is has the potential for the most dynamic range and hence most contrast (**Figure 2**). However, M_Z after the pulse is dependent on M_Z immediately prior to the pulse (it will be the same magnitude but point in the opposite direction). This means that the length of the previous inversion time (TI) will affect the magnitude of M_z after inversion pulse. In a gated cardiac scan, the TI is roughly equal to the RR interval. This makes scans with IR preparation very sensitive to changes in heart rate and arrhythmias because the RR and TI change throughout the scan. The other disadvantage of IR is that it requires a longer readout because it takes longer for the magnetization to recover. Practically, this means that more time is required per slice, so fewer slices can be acquired, and there is a decrease in spatial coverage.

Currently, the majority of CMR perfusion scans are acquired using SR preparation. While there is less dynamic range and contrast because it is only a 90 degree pulse (see **Figure *2***), SR does not have the other drawbacks of IR. Critically, SR pulses will always set M_z to zero regardless of the prior M_z, so the signal has no heart rate dependence. Additionally, because the readout is faster, more slices can be acquired allowing for greater spatial coverage.

Other pulse preparations are currently being developed. Some, like magnetization driven steady state, offer better linearity at the expense of CNR, which may be useful for some quantification applications. Others are a hybrid of SR and IR preparations. For example, an SR prep followed

by an IR prep[13] will exhibit some characteristics of each. There will be no heart rate dependence, and CNR will be improved over a simple SR prep, but readout would take even longer and coverage would decrease. This could be used in cases where good CNR is important but coverage is not (e.g. a diffuse process like systemic sclerosis).

For a 90 degree SR preparation, there are a few different choices for how to implement the RF pulse. A rectangular pulse is the simplest, however in the presence of any B1 field inhomogeneity (common in cardiac imaging) a rectangular pulse will result in incomplete saturation. Other RF pulses have been designed that have improved performance in the presence of B1 inhomogeneity. Two important ones are adiabatic pulses [14] and rectangular pulse trains[15]. Both of these show markedly improved saturation[6, 15]. However their drawbacks are longer pulse durations and higher SAR. The longer pulse duration is minor compared the image acquisition time (~8ms compared to ~150-200ms), but additional SAR can be problematic with large coverage at higher field strengths (3T).

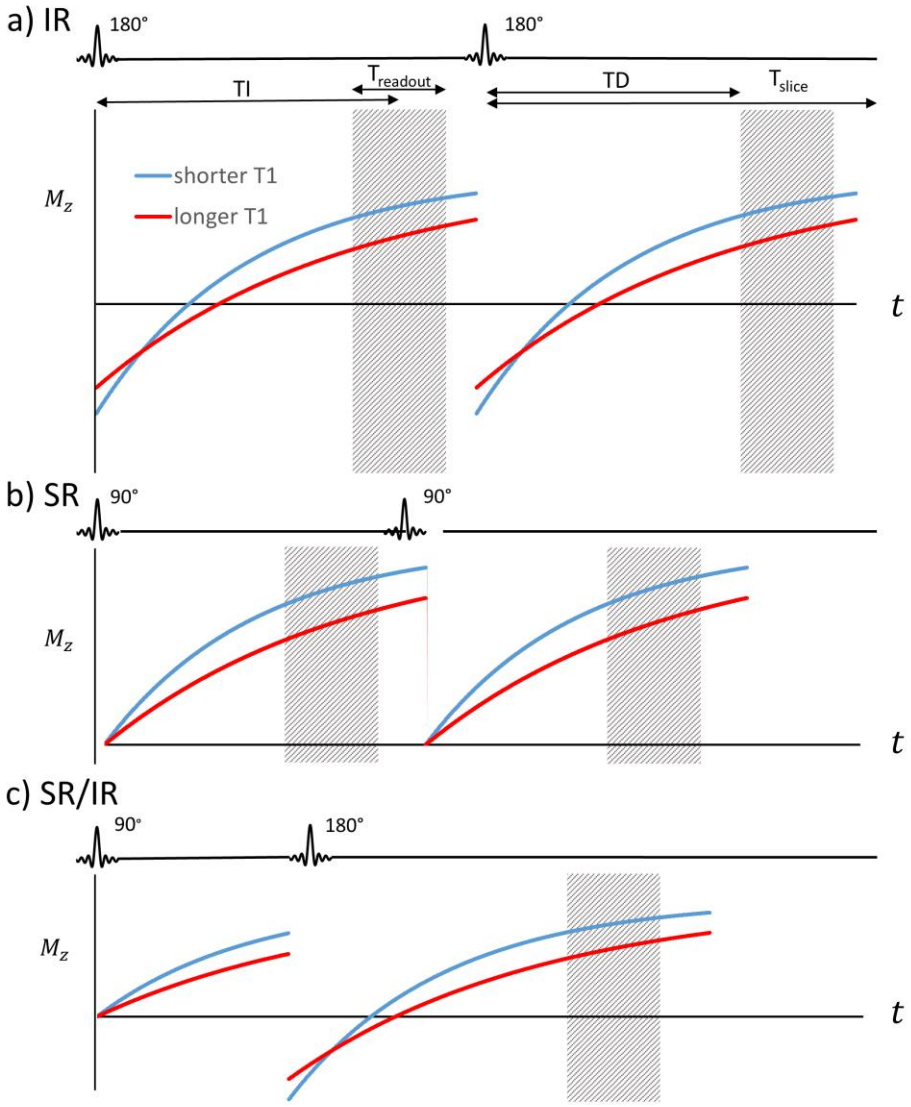

Figure 2: Preparation pulses for cardiac perfusion sequences
(a) Saturation recovery (SR), (b) inversion recovery (IR), and (c) hybrid SR-IR preparations for myocardial imaging. IR has a greater signal range but is slower and is susceptible to variations in heart rate (note that Mz after the inversion pulse is dependent on Tslice/T1). For the hybrid SR-IR, the initial SR preparation removes any heart rate variability, and the following IR pulse increases signal range over an SR only prep. TD = trigger delay, TI=inversion time (time from preparation to center of k-space), Treadout = total time for acquisition of all k-space data for a single slice, Tslice = total time required for acquiring a single slice. Note that TI is TD plus half Treadout.

1.2.3 Image readout: snapshot FLASH, SSFP, GRE- EPI

Each type of magnetization preparation pulse can be combined with different types of image readout. The most common types are ultra fast gradient echo (e.g. TurboFLASH, fast GRE, and Turbo Field Echo)[16], gradient echo with echo planar readout (GRE-EPI)[17], or steady state free precession (SSFP - e.g. TrueFISP, FIESTA, balanced FFE)[18], and despite much debate, there is no clear consensus for which sequence is best for CMR perfusion and is usually determined based on the preference of the physician.

Fast Low Angle Shot (FLASH) was one of the first available rapid imaging sequences. With FLASH, each line in k-space is preceded by a low flip angle excitation and then any transverse magnetization at the end of the readout is spoiled before moving to the next line (**Figure 3**). Since each line has its own excitation, the imaging time for the readout (not including preparation) will be $T_{readout} = TR * N_{phase}$. E.g. for a 128x80 matrix at TR=2ms, the readout time would be 160ms. (Note: TR here refers to time between excitations during the readout, it does not refer to the time between successive image acquisitions.) TurboFLASH is a variation on FLASH with very short TR and low flip angle. As a consequence, TurboFLASH is predominantly proton density weighted instead of having the typical T_1 FLASH weighting. However, with IR or SR prep a TurboFLASH sequence will have T_1 weighting.

GRE-EPI is similar to FLASH, except that instead of reading out one line of k-space per acquisition, multiple lines are read out. This means that fewer excitations are needed during readout, which makes GRE-EPI more efficient and hence faster than FLASH. The number of lines read per excitation is referred to as the echo train length (ETL). For GRE-EPI, the readout

time will instead be $T_{readout}$ = TR * N_{phase} / ETL. For example a 128x80 matrix at TR=6ms with an ETL of 4, the readout time would be 80*6/4 = 120ms. The imaging readout time is particularly important in CMR because motion artifacts are reduced with shorter readout times. This makes GRE-EPI less sensitive to motion than FLASH. Additionally, the faster readout time reduces the overall imaging time per slice, which means more slices can be acquired during each heartbeat. One drawback of GRE-EPI, however, is that magnetic field imperfections accumulate through the extended readout. The accumulation of error manifests itself as additional phase, which can mimic the intended phase used to localize signal within an image. The result is that EPI images exhibit phase related "ghosting" artifacts.

Steady State Free Precession (SSFP) images are a variant of FLASH. Unlike in FLASH, in SSFP transverse magnetization (M_{x-y}) is not eliminated before the next excitation. Rather than being destroyed (i.e. spoiled) by the application of phase-modulated RF pulses or large field gradients, the residual transverse magnetization is refocused and combined with newly excited transverse excitation to dramatically increase the magnetization used in the formation of an image (**Figure 3**). This gives SSFP greater signal to noise ratio (SNR) than either FLASH or GRE-EPI. Also, because initial magnetization depends on both the longitudinal magnetization and the refocused transverse magnetization, SSFP will have some T_2 as well as T_1 contrast. This makes TE particularly important for SSFP readouts. Like FLASH, SSFP requires one excitation per readout line, and has comparable readout times. Some studies have found more dark rim artifacts with SSFP [19, 20]. Magnetic field inhomogeneity, which can be problematic in the chest where the lungs impart large local magnetic susceptibility changes, is also a problem in SSFP readouts, which has limited SSFP adoption at 3T. It has also been reported that the

excitations in SSFP can interfere with accurate ECG gating[18]. Still, in spite of these drawbacks, the gain in SNR has seen SSFP become increasingly popular in CMR perfusion.

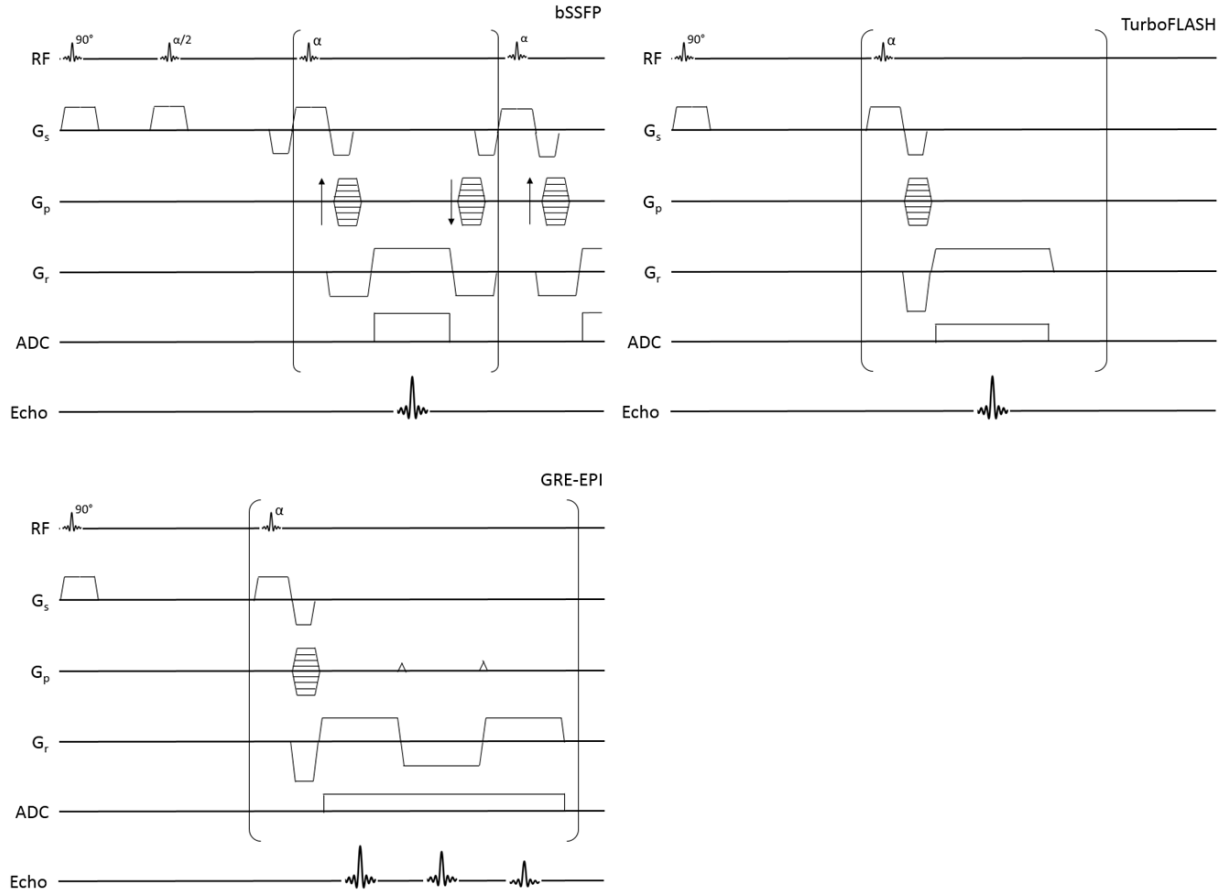

Figure 3: Pulse sequence diagrams for bSSFP, FLASH, and GRE-EPI readouts

1.2.4 Acquiring Multiple Slices

Typically CMR perfusion scans require multiple slices for adequate coverage of the areas supplied by the major coronary arteries. The most common method for acquiring multiple slices is to use multiple SR preps. The first slice is SR prepped and read out, then the second slice is SR prepped and read out, etc. until all the slices are completed. Another approach is to use a single SR prep and then read out multiple slices. This is faster than using multiple SR preps, so

greater spatial coverage is possible. However, the time between the SR prep and readout will be different for each slice. This leads to a very important disadvantage: each slice will have a different TI, so each slice will have different CNR. A third possibility is to use a single SR prep but interleave the slice readouts. This keeps the same efficiency gains but equalizes the TIs, so there is no CNR variation between slices. However, the readout per slice is longer, which increases susceptibility to motion artifacts.

1.2.5 Acceleration Techniques

Due to the need for very fast image acquisition, cardiac perfusion sequences are almost always run with some sort of acceleration technique. Acceleration techniques include parallel imaging (e.g. SMASH[21], SENSE[22], and GRAPPA[23]), k-t Blast/k-t SENSE[24], and HYPR[25, 26]. Much research has been focused on acceleration techniques in recent years, and a multitude of techniques have been developed and compared[27, 28]. In all of these techniques, image acquisition time is reduced by intentionally sampling only a subset of the data needed to create an MRI images. The uncollected or "missing" MRI data are mathematically synthesized using complimentary information collected from different receiver coils. In other words, most acceleration techniques use the spatial location of the acquired signal which is inherent in the receiver coil configuration to reduce the amount of imaging data that must be acquired for artifact free images. Since receiver coil information is acquired simultaneously, i.e. in parallel, the general approach to acceleration is referred to as "parallel imaging". However, a major tradeoff in all cases is that faster acquisition results in lower SNR. A review of parallel imaging basics can be found by Deshmane et al[29].

Sensitivity encoding (SENSE) and generalized autocalibrating partially parallel acquisition (GRAPPA) are two widely available methods of parallel imaging, and both have major advantages in that they rely on relatively simple theoretical underpinnings and make very few assumptions about the nature of the underlying images. With parallel imaging, reconstruction additionally incorporates information from multiple independent receiving coils. In essence, spatial information that would otherwise be obtained by spatial encoding via gradients is instead obtained by information in independent coils in the receiver coil array. With SENSE, coil sensitivity profiles are used to unwrap the aliased images in image space. With GRAPPA, the unsampled lines in k-space are calculated by combining information from neighboring lines in multiple coils, and the filled-in k-space is then reconstructed as usual. This eliminates the ghosting artifacts that would normally be seen by undersampling, and the more receiving channels that are used, the more k-space can be undersampled and acquisition speed increased. Other techniques achieve even greater acceleration by incorporating temporal information. For most rapidly acquired image series of the heart, much of the image remains unchanged between images, and data is correlated in time. k-t BLAST and k-t SENSE are two well-known techniques that take advantage of this correlation by acquiring a training data set (acquired at low resolution and un-aliased) that is used to inform the reconstruction of the sparsely sampled and rapidly acquired data. k-t BLAST does not incorporate coil channel information in its reconstruction and can be used with single channel coils whereas k-t SENSE incorporates coil channel information as well. Compared to standard parallel imaging techniques, k-t BLAST and k-t SENSE are capable of faster imaging, but at the cost of increased noise and more assumptions in the model (e.g. that motion during the training data is representative of motion in the rest of the data).

1.2.6 Motion Correction

While many cardiac MRI scans rely on breath holds to ensure that there is minimal movement of the heart during the scan, the longer acquisition times of a cardiac perfusion scan (typically 45s – 1.5min) can make breath holds impractical. As a result, there is usually considerable cardiac motion over the course of a perfusion scan. This is problematic when analyzing perfusion images. Generating signal intensity time curves requires segmenting along the epi- and endocardial borders, but this is an extremely time intensive process to do frame by frame, and automatic segmentation often does not trace the borders well. A more efficient process is to first register all of the images together, draw the contours on a single image, and then propagate the contours throughout the series and make (relatively minor) adjustments as needed. As such, most cardiac perfusion scans will include some form of motion correction for image registration. There are a multitude of motion corrections algorithms that have been proposed. Motion can be corrected prospectively using navigator pulses that track the motion of the diaphragm[30]. Motion can also be corrected retrospectively using a variety of methods[31-34]. In practice, many vendors will have some form of inline motion correction included in their cardiac sequences. A comprehensive review of cardiac motion correction can be found in the review by Scott et al[35].

1.2.7 Artifacts

There are several artifacts seen in CMR perfusion imaging, and the most important one is the dark rim artifact (DRA). The DRA manifests as a dark rim that is sometimes seen in the subendocardial border of the ventricle. This ring can easily be mistaken for hypoperfusion and cause incorrect diagnoses, which is why DRA is regarded as the most concerning artifact in

CMR. Much research has gone into determining the cause of the DRA, and some common hypotheses include Gibbs ringing, contrast associated susceptibility changes, motion artifacts, and partial volume effects[36]. However, no theory has been clearly identified as the sole cause of DRA, and its origins remain widely debated.

1.2.8 1.5T vs 3T

While the majority of clinical scanners use 1.5T magnets, 3T is becoming increasingly common, and the choice between the two has a significant effect on CMR perfusion. The higher magnetic field of the 3.0T results in a doubling of the signal-to-noise ratio of images and a 30% prolongation of T1 values and a shortening of T2 values[37]. Importantly, Gadolinium-based contrast agents have less relaxivity at 3T. However, since T_1 values are also higher in the blood and myocardium at 3T than at 1.5T there is a net increase in ΔT_1 and gain in CNR[38]. While 3T offers CNR advantages, it has other disadvantages. Artifacts are more prominent at 3T, though faster imaging and higher bandwidth can mitigate artifacts at the cost of SNR. Critically for SSFP sequences, there is more inhomogeneity at 3T [39]. There is also greater energy deposition as quantified by the Specific Absorption Rate (SAR) at 3T, which limits the TR and flip angles that can be used, and ECG signal is noisier at 3T, which can influence any scan where accurate gating is critical.

1.2.9 Summary

There are a multitude of choices available when creating a CMR perfusion sequence. Preparation can be IR, SR, or a hybrid, and there are multiple ways to implement the preparation. Readouts can be some variation of FLASH, GRE-EPI, or SSFP. There is no single best

combination for all applications, and selection of the "best" sequence depends on the specific needs of a particular scan. For example, relative to ischemia, post infarction imaging involves more microvascular than macrovascular obstruction, so contrast washes out more slowly[8]. In this case, some temporal resolution could be sacrificed to gain greater spatial resolution to better delineate the size of injured myocardium. Conversely, for a diffuse process like microvascular dysfunction in Syndrome X, spatial coverage could be neglected in favor of having greater spatial resolution in fewer slices to evaluate subendocardial hypoperfusion.

1.3: First Pass Perfusion Analysis

After image acquisition, the data must be processed to convert signal vs time curves into perfusion measurements. Broadly speaking, perfusion analysis can be categorized as qualitative, semi-quantitative, or absolute quantitative.

1.3.1 Qualitative

The simplest way of analyzing perfusion data is to simply visually inspect myocardial signal changes as the bolus of contrast agent passes, which is what is done in most clinical applications. A physician will cycle through the perfusion series and watch the myocardium as the contrast flushes through. Any areas that remain dark have less perfusion than the surrounding bright tissue. Comparison of stress, rest, and late gadolinium enhanced images allows defects to be attributed to ischemia, infarction, or artifact. Defects seen at stress but not at rest are interpreted as reversible ischemia. Matched defects seen at stress and rest with a corresponding area of late gadolinium enhancement are interpreted as infarction. Matched defects seen at stress and rest

without any late gadolinium enhancement are interpreted as artifact. This algorithm improves the diagnostic accuracy over interpretation of the perfusion images alone[40].

1.3.2 Semi-Quantitative

Broadly speaking, semi-quantitative approaches result in numeric indices of perfusion, but the units of the measurement are not synonymous with blood flow (i.e. not ml/min/g). For example, the qualitative approach described above could be modified by comparing the change in signal in diseased myocardium verses the change in signal in healthy myocardium in the same subject. While this ratio will give a numeric value, it will not be units of blood flow. In general, while semi-quantitative approaches do allow for some statistical comparisons to be made, they are still limited compared to a true quantitative approach. The measurements themselves often depend on non-flow related parameters such as contrast dose or coil sensitivity, so there can still be problems comparing across subjects and over time. Additionally, because units are not in ml/min/g, direct comparisons cannot be made to other imaging modalities that are truly quantitative (e.g. PET). Common semi-quantitative measures include max upslope during the wash-in period and the area under the curve during the wash-in period.

1.3.3 Absolutely Quantitative

Absolute quantification approaches aim to measure not just a perfusion related parameter but an exact measurement of perfusion in ml of blood, per minute of time, per gram of myocardium (ml/min/g). These approaches all make use of kinetic modeling and input functions.

The fundamental model for quantitative perfusion imaging in any organ system is

$$C(t) = Q \cdot \big(AIF(t) \otimes R(t)\big) \quad (1)$$

Where *C(t)* is the contrast in the myocardium, *Q*is the myocardial blood flow, *AIF(t)* is the arterial input function, and *R(t)* is the tissue residue function (**Figure 4**). AIF(t) is the contrast in the feeding artery, so Q · AIF(t) describes the amount of contrast that is flowing into the myocardium. Ideally, the AIF would be measured in the coronary arteries, but their small size makes this impractical, so in CMR perfusion, the AIF is sampled at the left ventricle. The tissue residue function, R(t), is a measure of contrast retention in the myocardium. R(t) can also be thought of as the myocardial response to a short bolus of contrast directly in the feeding artery, and it is analogous to an impulse response function. $\otimes$ is the convolution function, defined by

$$f(t) \otimes g(t) = \int_{-\infty}^{\infty} f(t)g(t-\tau)d\tau \quad (2)$$

The aim of absolute quantification is to solve the first equation for *Q*. However, only *C(t)* and *AIF(t)* can be measured directly. To find *Q*, *R(t)* must be found by deconvolving *AIF(t)* from *C(t)*.

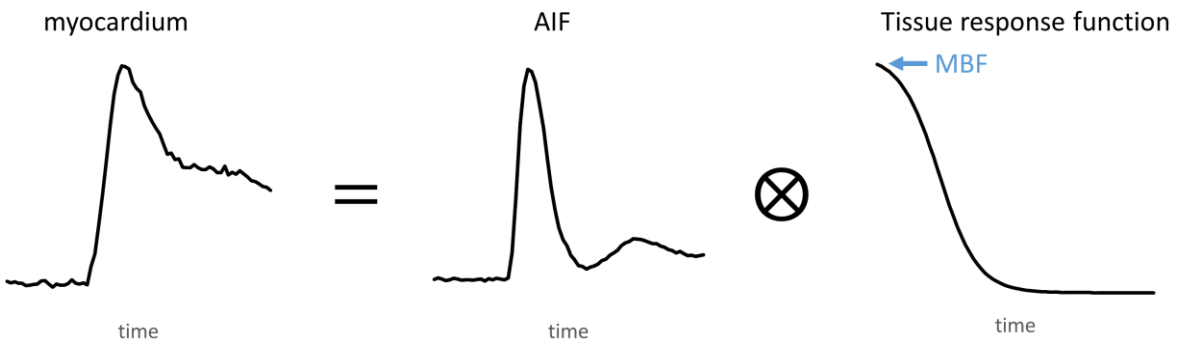

Figure 4: Tissue contrast as a function of AIF and residue function
Contrast concentration in the myocardium is the convolution of the arterial input function (AIF) and a tissue response function. Depending on the model used, the maximum value of the tissue response function can be equivalent to the blood flow. Blood flow is calculated by deconvolving the AIF to find the tissue response function.

There are a number of ways to do this deconvolution, but the most common ones used in cardiac perfusion are the two-compartment and Fermi models. The two-compartment model[41] starts by using the Tofts model to describe the rate of change of myocardial contrast concentration

$$\frac{dC(t)}{dt} = K^{trans} AIF(t) - k_{ep} C(t) \quad (3)$$

Where K^{trans} is the rate constant of contrast transfer from the vasculature to the interstitial space and k_{ep} is the rate constant of contrast transfer from the interstitial space to the vasculature. Solving for C(t) yields

$$C(t) = AIF(t) \otimes K^{trans} e^{-k_{ep} t} \quad (4)$$

which models the myocardial contrast as a function of *t*, K^{trans}, k_{ep}, and *AIF(t)*. By comparing the *C(t)* in Equation 4 to the *C(t)* measured in an MRI experiment, K^{trans} and k_{ep} can be calculated by standard least squares minimization methods such as a Levenberg-Marquardt algorithm or trust region reflective algorithm (the default used in MATLAB). Put another way:

$$\{K^{trans}, k_{ep}\} = \min_{K^{trans},k_{ep}} \left(\sum_t \left(C(t) - AIF(t) \otimes K^{trans} e^{-k_{ep}t} \right)^2 \right) \quad (5)$$

Once K^{trans} is determined, blood flow (Q) can be calculated using the equation

$$K^{trans} = QE \quad (6)$$

Where E is the extraction fraction and accounts for gadolinium leakage from the vasculature to the myocardium. Determining E is not trivial, and in real life E varies with blood flow and can be different under rest vs stress conditions [42]. Practically, an E value is usually assumed, and error introduced by this assumption is a major drawback of the two-compartment model.

The Fermi model works analogously to the two-compartment model except it uses the following form for *R(t)*:

$$R(t) = \frac{A}{e^{k(t-\Delta t)} + 1} \quad (7)$$

Similar to how the two-compartment model is solved, the variables in the Fermi model can be solved for by substituting Equation 7 into Equation 1 and minimizing the difference between the model and the measured signal:

$$\{A, k, \Delta t\} = \min_{A,k,\Delta t} \left(\sum_t \left(C(t) - AIF(t) \otimes \frac{A}{e^{k(t-\Delta t)} + 1} \right)^2 \right) \quad (8)$$

Once the model parameters k, A, and Δt are solved for, blood flow can be calculated by evaluating Equation (7) at $t = \Delta t$.

1.4: Current AIF Saturation Correction Methods

Accurately deconvolving the AIF and finding the correct residue function requires an accurate sampling of the AIF. While it is easy to locate the AIF in CMR – it is easily sampled in the LV – it is difficult to accurately capture the correct shape of the AIF. First, the AIF peak is very sharp since the contrast passes through the LV so quickly, and most acquisition schemes will miss the exact top of the peak. To account for this, many processing algorithms assume the AIF is described by a gamma variate function [43] and will use the sampled AIF data to fit a continuous gamma variate that is then used in the rest of the algorithm. Second, because the concentration of contrast is so high in the LV during the first pass of the bolus, there are significant saturation and T_2* effects, which manifest as flattening the measured AIF. For an SR-TurboFLASH sequence, the signal equation (for the central k-space line) is as follows:

$$S = S_0 \left[(1 - e^{-R_1 TD}) a^{N/2-1} + (1 - E_1) \frac{1 - a^{N/2-1}}{1 - a} \right]$$

where $a = E_1 \cos \alpha$ and $E_1 = e^{-R_1 TR}$. At low R_1, signal vs R_1 is approximately linear. At high values of R_1, which are reached during the peak of the AIF, the signal deviates from the linear approximation (**Figure 5**).

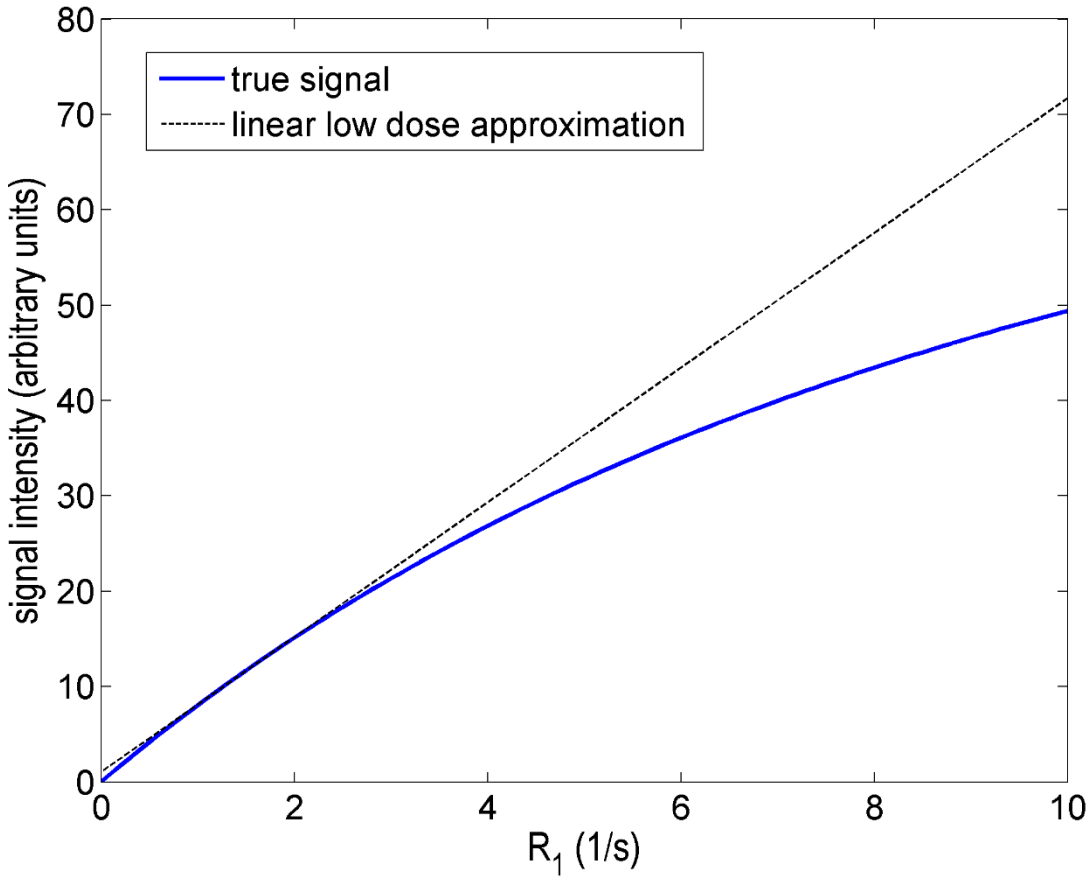

Figure 5: Signal vs R1 for a SR-TurboFLASH sequence
Signal intensity of central k-space lines vs R1 for a SR prepared FLASH sequence using typical parameters. For low doses of contrast, the signal response is linear, but at higher doses there is significant non-linearity.

The AIF saturation problem is much difficult to correct, and there have been a number of proposed methods to remedy it. While they are all different in approach, the common theme throughout is trading signal intensity (and with it SNR) for signal linearity.

1) **Low contrast dose**. The simplest way to avoid AIF saturation is to simply use less contrast agent, which reduces signal intensity and hence improves linearity. While the SNR loss in the AIF is typically acceptable, the accompanying loss of SNR in the myocardium is problematic. This is especially true in a clinical environment where

myocardial SNR loss makes qualitative interpretation more difficult, which is the mainstay of clinical perfusion interpretation

2) **Dual bolus** [44]. Dual bolus also uses a low concentration contrast dose, but as the name implies it also uses a normal concentration contrast dose in a separate acquisition. The AIF is taken from the low dose and the myocardial signal from the regular dose. While this seems to capture the best of both worlds, in practice having two separate scans is difficult to implement and introduces a lot of experimental error. This may explain why despite having been introduced in 2004 there has not been widespread adoption of this technique.
3) **Prebolus** [45]. Prebolus is similar in concept to dual bolus but instead of using a dilute bolus to capture the AIF, it uses a small volume of normally concentrated contrast. Adoption of prebolus has also been limited.
4) **Dual echo** (also sometimes referred to as "dual sequence") [46]. Unlike the other methods, dual echo requires no change in contrast dosage or strength. Instead, an extra low resolution, low SNR image is acquired during each heartbeat that is used to capture the AIF. While dual echo has a major advantage of ease of use since it requires no changes in physical setup, unlike dual bolus dual echo has never been directly validated against gold standard measurements, and so far only relative perfusion values (in MPR) have been reported.

1.5: "Bookend" Quantitative Perfusion

As noted in the previous section, despite the fact that a number of different methods for quantifying myocardial perfusion have been proposed, none of them are widely available or used clinically. However, our lab has developed a method for *cerebral* perfusion called "Bookend" perfusion that has been validated against gold standard measurements and is simple to use from a user standpoint [47-51]. No additional work is needed by the person performing the scan; fully quantitative maps (in ml/min/g) are generated automatically by the sequence reconstruction. This method has been refined and optimized and is used regularly at our institution's hospital. If this same method could be applied to myocardial perfusion, it might provide a simple, turn-key quantitative myocardial measurement that can be used in clinical environments.

In short, Bookend perfusion works by calculating the blood *volume* from first-pass data, re-calculating blood volume data from a steady state T_1 sequence, and then comparing these two measurements to create a correction factor that can be applied to the blood flow measurements.

To calculate blood volume from first-pass data, the typical gadolinium contrast agent must be substituted with some type of intravascular contrast agent so that it cannot leave the intravascular space. The tissue residue function is calculated from Equation 1, but rather than use explicit model such as two-compartment or Fermi, a model-independent method is used to find *R(t)*. There are several ways to do this, but a common is to use singular value decomposition (SVD). This residue function has two important properties: 1) its maximum value is equal to the blood flow and 2) the area under the function is equal to the blood volume. However, as in the cases

above, these blood flow and blood volume measurements are incorrect because they are calculated using a saturated AIF.

Next, blood volume is calculated from steady state T_1 data. In short, the first-pass sequence is "bookended" by two modified Look-Locker (MOLLI) T_1 sequences, and the relative changes in T_1 in the blood pool vs myocardium can be used to calculate blood volume. Because no AIF is used, this blood volume measurement does not suffer the same saturation problems and is much more accurate than the blood volume calculated from the first-pass data. This process is described in much greater detail in the next chapter of this dissertation.

Finally, these two blood volume measurements are used to derive a correction factor that is applied to the blood flow data. The correction factor, *CF*, is defined as

$$CF = \frac{qMBV}{MBV_{FP}} \tag{9}$$

where $qMBV$ is the quantitative myocardial blood volume calculated from the steady state T1 data and MBV_{FP} is the myocardial blood volume calculated from the first-pass residue function. This correction factor is assumed to be resulting principally from the incorrectly measured AIF and is assumed to be equally applicable to blood flow measurements. Quantitative blood flow can then be calculated as

$$qMBF = CF * MBF_{FP} \tag{10}$$

where $qMBF$ is quantitative myocardial blood flow in ml/min/g and MBF_{FP} is myocardial blood flow calculated from the first pass data.

Chapter 2: Myocardial Blood Volume and Water Exchange

2.1: Introduction

The first step in adapting Bookend perfusion to the myocardium is to develop a way to quantify steady state myocardial blood volume (MBV) so that it can be used to calculate a correction factor as shown in Equation (9). Additionally, aside from its potential role in improving perfusion quantification, MBV may be itself be an important biomarker for disease. Studies have shown that MBV decreases are associated with capillary closure on histological section[52-54], and it could reasonably be hypothesized that diseases known to cause microvascular changes would show an associated decrease in measured MBV. While there has not been much research in this area, one contrast ultrasound study[55] has shown that MBV is a marker of cardiac allograft vasculopathy (CAV), a disease that is known to cause microvascular dysfunction. Additionally, an animal study [56] has shown that blood volume reserve measurements are similarly predictive of coronary artery disease (CAD) as perfusion reserve measurements, and furthermore they may be better able to differentiate between moderate and severe stenosis than perfusion reserve measurements. Even if the MBV measurements had no improved diagnostic value over perfusion measurements, being able to use MBV instead of perfusion would be of enormous value in clinical workflow. Because MBV is imaged in steady state instead of during first-pass, there is no risk of missing the timing window and having uninterpretable data. Additionally, the largest bottleneck in perfusion analysis is in contouring the endocardial and epicardial borders in each scan. While a perfusion sequence may have upwards of 60 images to contour, calculating MBV only requires contouring a single pre-T_1 and post-T_1 image. This

represents a massive decrease in the time necessary to analyze data, which could have a large impact on clinical workflow. In spite of this diagnostic potential for MBV measurements, to date it has been mostly studied in animals [56-58] and has received scant attention in human studies. While this may be due to lack of interest by the research community, it may also be due in part to the deceptive difficulty of calculating quantitative MBV, and without attention to detail it is very easy to arrive at incorrect MBV values.

While myocardial blood volume has not had much attention in research, extracellular volume fraction (ECV) has been well studied and has been shown to be an important marker of disease[59]. Here we use the same principle of comparing blood vs tissue relaxivity changes as is used in ECV calculation, but by using an intravascular contrast agent (ferumoxytol) instead of gadolinium we are able to calculate MBV instead of ECV. However, even if the contrast agent is intravascular, water is free to move across the vascular wall. Water can move from the extravascular space into the intravascular space, interact with contrast, and then move back to the extravascular space. Unless accounted for, these water-exchange effects can introduce substantial error into MBV measurements [60]. Presented here is a method for measuring MBV and exchange rates using a Hazlewood two-compartment model. We then validate this model in a volunteer cohort, demonstrating a method for accurately quantifying MBV in human subjects. Finally, we use a subset of these subjects to demonstrate the potential of using quantitative MBV measurements to improve myocardial perfusion measurements.

2.2: Mathematical Model

2.2.1 Initial MBV measurement by relaxivity changes

For our initial measurement of MBV, we use a method identical to that used for measuring ECV. In this model, we model the myocardium as a two compartment system consisting of an intravascular and extravascular compartments. A T_1 image is acquired using a MOLLI sequence before any contrast is injected and then another T_1 image is acquired after contrast injection. Then change in relaxivity (R_1, defined as $1/T_1$) in the blood pool and myocardium after contrast injection can be described as a function of the contrast agent concentration:

$$\Delta R_1^{LV} = r_1 c_1^{LV} \tag{10}$$

$$\Delta R_1^{myo} = r_1 c_1^{myo} \tag{11}$$

Where ΔR_1^{LV} and R_1^{myo} are relaxivity changes in the left ventricle and myocardium, c_1^{LV} and c_1^{myo} are the contrast agent concentrations in the left ventricle and myocardium, and r_1 is the relaxivity constant of the contrast agent. Here, we assume that the intravascular and extravascular compartments are well mixed and that relaxation can be simply described by the weighted average contrast concentration of the two compartments. Assuming that the contrast agent is confined to the vascular compartment and that there is no difference in hematocrit concentration between the left ventricle and myocardium, we can express the contrast agent concentration in the myocardium in terms of the left ventricular concentration and the MBV:

$$c_1^{myo} = c_1^{LV} * MBV \tag{12}$$

Simple substitution and rearrangement yields MBV as a function of the measured relaxivity changes:

$$MBV = \frac{c_1^{myo}}{c_1^{LV}} = \frac{\Delta R_1^{myo}}{\Delta R_1^{LV}} \tag{13}$$

In an ideal case, this would be all that is needed to calculate MBV, but in reality water exchange complicates this measurement.

2.2.2 Signal Equation corrected for water exchange

Implicit in Equation 11 is the assumption that relaxivity of the myocardium can adequately be described as a single weighted average of the relaxivity of the intravascular and extravascular components. This would be the case if the intra- and extravascular compartments could be treated as a single well-mixed compartment, but in reality the degree of mixing is governed by the speed at which water transverses the vascular wall. This phenomenon was first described by Hazlewood[61]. Hazlewood described the magnetization of a compartment as not only a function of the compartment's relaxivity but also as a function of proton flow in and out of the compartment. In the context of the myocardium, these equations would be

$$\frac{d\Delta M_{blood}}{dt} = -\frac{\Delta M_{blood}}{T_1^{blood}} - \frac{\Delta M_{blood}}{\tau_{blood}} + \frac{\Delta M_{EV}}{\tau_{EV}} \tag{14}$$

$$\frac{d\Delta M_{EV}}{dt} = -\frac{\Delta M_{EV}}{T_1^{EV}} - \frac{\Delta M_{EV}}{\tau_{EV}} + \frac{\Delta M_{blood}}{\tau_{blood}} \tag{15}$$

Where ΔM_{blood} and ΔM_{EV} are the difference in longitudinal magnetization from equilibrium in the blood and extravascular spaces. τ_{blood} is the average residence time of a proton in the blood compartment before it traverses to the extravascular compartment, and τ_{EV} is the average residence time of a proton in the extravascular compartment before traversing to the blood compartment. In these equations, magnetization change is described as the total change due to compartment relaxivity (first term), protons leaving the compartment (second term), and protons entering the compartment (third term). These equations can be constrained by requiring that there is no net proton movement:

$$\frac{f_{blood}}{\tau_{blood}} = \frac{f_{EV}}{\tau_{EV}} \tag{16}$$

$$f_{blood} + f_{EV} = 1 \tag{17}$$

f_{blood} and f_{EV} are the fraction of protons residing in the blood and extravascular compartments. Together, these equations and constraints can be solved for to yield equations describing the net change in magnetization in equilibrium as a function of time.

In the absence of any water exchange, the signal equation for an inversion recovery sequence sampling two compartments can be written as

$$S(t) = M_0 f_{blood}\left(1 - 2e^{-t/T_1^{blood}}\right) + M_0 f_{EV}\left(1 - 2e^{-t/T_1^{EV}}\right) \tag{18}$$

Donahue[60] combined the Hazlewood equations with the inversion recovery signal equation to yield a modified signal equation that incorporates water exchange effects. In the myocardium, this equation can be written as

$$S(t) = M_0 f'_{blood}\left(1 - 2e^{-t/T'_{blood}}\right) + M_0 f'_{EV}\left(1 - 2e^{-t/T'_{EV}}\right) \quad (19)$$

$$\frac{1}{T'_{blood}} = C_1 + C_2 \quad (20)$$

$$\frac{1}{T'_{EV}} = C_1 - C_2 \quad (21)$$

$$f'_{EV} = 1 - f'_{blood} \quad (22)$$

$$f'_{blood} = \frac{1}{2} - \frac{1}{4}\left[(f_{EV} - f_{blood})\left(\frac{1}{T_1^{blood}} - \frac{1}{T_1^{EV}}\right) + \frac{1}{\tau_{blood}} + \frac{1}{\tau_{EV}}\right]/C_2 \quad (23)$$

$$C_1 = \frac{1}{2}\left[\frac{1}{T_1^{blood}} + \frac{1}{T_1^{EV}} + \frac{1}{\tau_{blood}} + \frac{1}{\tau_{EV}}\right] \quad (24)$$

$$C_2 = \frac{1}{2}\left[\left(\frac{1}{T_1^{blood}} - \frac{1}{T_1^{EV}} + \frac{1}{\tau_{blood}} - \frac{1}{\tau_{EV}}\right)^2 + \frac{4}{\tau_{blood}\tau_{EV}}\right]^{1/2} \quad (25)$$

Looking at Equation 19, it is apparent the signal equation including water exchange is structurally the same as the no-exchange signal equation except it uses modified values for T_1 and volume fractions

2.2.3 Effect of water exchange on MBV measurements

We can now model the myocardial signal during inversion recovery experiment. By evaluating Equation 19 at timepoints corresponding to the inversion times in a MOLLI sequence, we can simulate that datapoints that would be measured in a MOLLI sequence for a given τ_{blood} and f_{blood}. We then fit these datapoints using a mono-exponential function as is used for MOLLI sequence fitting. This fitting yields a "myocardial T_1" that we would expect to measure in the

setting of water exchange. Together, these steps describe a way of simulating the T_1 that would be measured as a function of the extravascular T_1, blood T_1, exchange rates, and MOLLI sequence parameters. This is summarized in **Figure 6**.

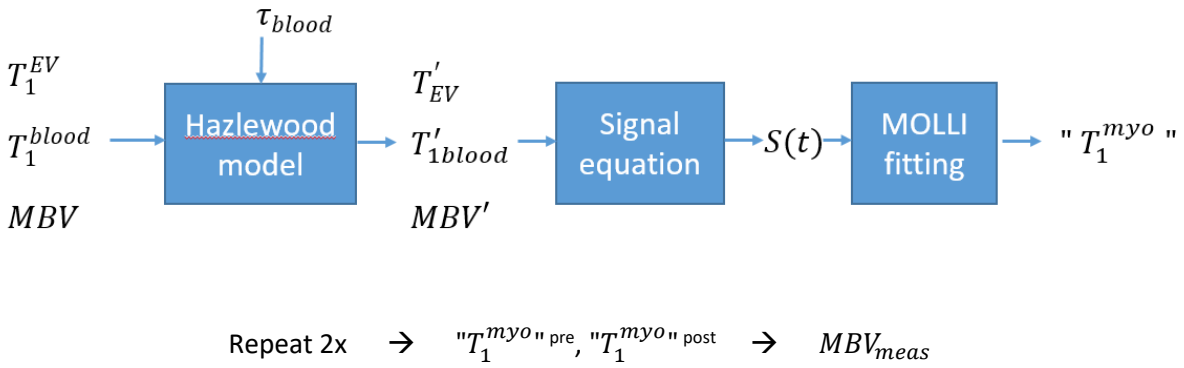

Figure 6: Model for simulating measured MBV
The T_1 values of the blood (measured in the LV) and extravascular space (assumed to be ~1000ms because no contrast is present) are input into the Hazlewood model along with and MBV and blood exchange frequency. This allows for calculation of a signal equation, which is then fitted to determine a T_1 value as if it were a simple mono-exponential function. Repetition of this model using pre-and post-contrast blood pool T_1 values allows for calculation of the expected measured MBV as a function of true MBV, τ_{blood}, and ΔT_1^{blood}.

By performing the above simulation twice, once with a pre-contrast T_1^{blood} and once with a post-contrast T_1^{blood}, and using Equation 13 we can simulate the MBV that we would expect to measure as a function of the exchange rates, fractional volumes, and change in blood pool relaxivity. Because MBV is synonymous with f_{blood}, this effectively defines the MBV we would expect to measure as a function of the real MBV:

$$MBV_{meas}^{sim} = g\left(MBV_{true}, \Delta R_1^{blood}, \tau_{blood}\right) \tag{26}$$

Where g represents the simulation described above and MBV_{meas}^{sim} is the MBV we would expect to measure according to the simulation. An example of the MBV_{meas}^{sim} as a function of ΔR_1^{blood} is

shown for various exchange rates in **Figure 7**. As seen in the figure, the greater the change in blood pool relaxivity and the shorter the exchange rate, the more difference there is between the actual and measured MBV. Unfortunately, higher contrast doses are preferred to maximize SNR, so **Figure 7** illustrates a tradeoff between MBV accuracy and SNR. However, the curves shown in **Figure 7** can also be used to correct for water exchange by a slight modification of the experimental protocol.

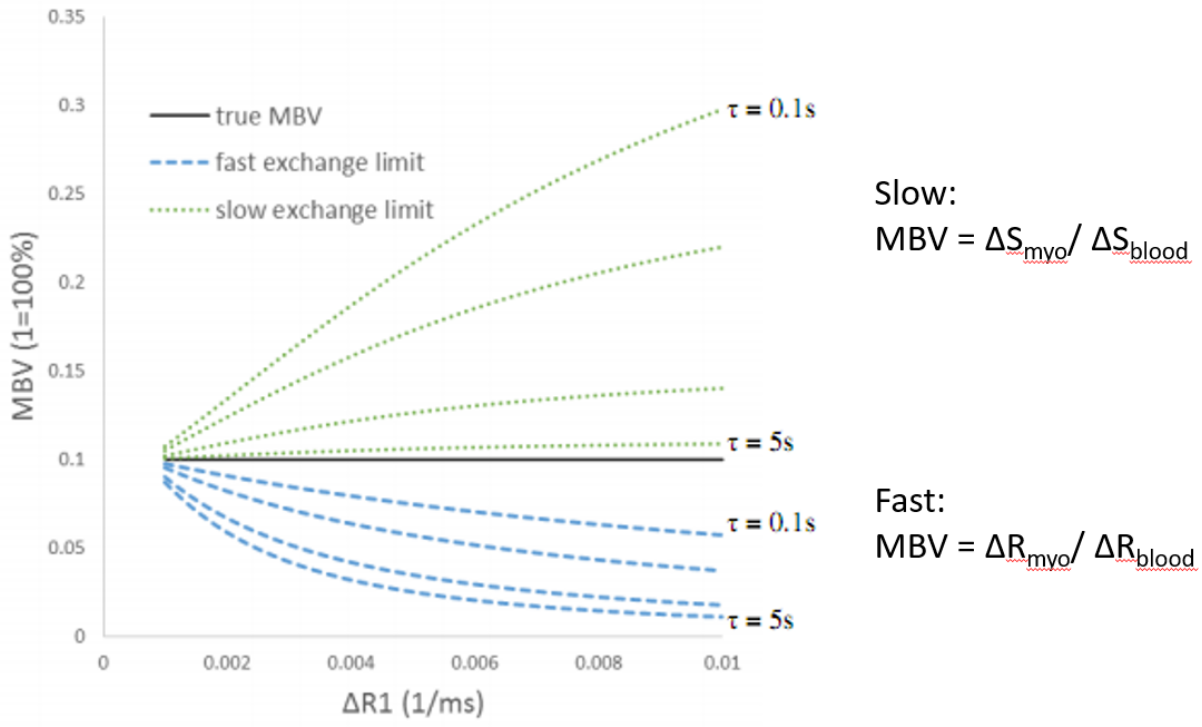

Figure 7: Water exchange model
Measured MBV in the slow and fast exchange limits are plotted as a function of blood pool relaxivity change for a true MBV of 10%. Typical measurements assume a well mixed single compartment, which corresponds to the fast exchange limit. As blood pool relaxivity increases, water exchange causes an increasingly large underestimation of the true MBV.

2.2.4 Measuring water exchange and true MBV

Figure 7 shows that for a given true MBV and exchange rate, there is a characteristic curve that describes the measured MBV as a function of change in blood pool relaxivity. By making several serial MOLLI measurements and comparing them to a baseline pre-contrast MOLLI, we can collect several data points of blood pool relaxivity change and measured MBV. Determining the exchange rate and true MBV then becomes a standard curve fitting problem where an exchange rate and MBV are chosen that minimizes the difference between the observed and simulated MBV measurements. Using least squares minimization, this approach can be described with the following equation:

$$\{\tau_{blood}, MBV_{true}\} = \min_{\tau_{blood}, MBV_{true}} \left(\sum_{\Delta R_1^{blood}} \left(MBV_{meas}^{sim} - MBV_{meas}^{obs} \right)^2 \right) \quad (27)$$

Where MBV_{meas}^{sim} is the simulated measured MBV as described by Equation 26 and MBV_{meas}^{obs} are the actual observed MBV measurements. In short, by taking several serial measurements of MBV at different contrast doses, the true MBV and exchange rates can be determined by using the measured MBV to map out one of the curves in **Figure 7**.

2.3: Selection of Contrast Agent

Critical to measuring MBV is using an intravascular contrast agent. Unfortunately, all of the widely used commercial contrast agents are gadolinium based agents that are known to leak across the vascular wall.

Initially, we attempted to use gadofosvaset (Ablavar) as an intravascular agent. Like all other major MRI contrast agents, Ablavar is a gadolinium based contrast agent and in its natural state is free to cross the vascular wall. However, unlike other agents, Ablavar binds to albumin in the blood. Once bound to albumin, Ablavar is unable to traverse the vascular wall, effective rendering it an intravascular agent. This property makes Ablavar well suited for certain types of angiography, and it has been approved by the FDA for use in MR angiography to evaluate aortoiliac occlusive disease. We sought to take advantage of these unique properties to measure MBV.

Unfortunately, Ablavar did not perform as expected in the myocardium. Earlier iterations of the experiments described below using Ablavar yielded very fast exchange rate and MBVs in the 20-30% range[62]. This is in inconsistent with the moderately slow exchange rates and 8-15% MBV values reported in animal studied [56-58]. Ultimately, we hypothesized that Ablavar was acting as an intravascular agent on first pass and that the high "MBV" was actually an ECV and that the fast exchange rate was between the extracellular and intracellular compartments, not the extravascular and intravascular compartments. After examining the literature, we discovered a study performed in rabbits that showed the bound fraction of Ablavar as a function of time after injection[63]. Notably, it took 10 seconds before 50% of the Ablavar bound to albumin. Because first-pass imaging takes soon after contrast injection, it is possible that during first-pass the ablavar is not yet bound to albumin and leaks into the myocardial extracellular space. This would explain the apparent discrepancy between our results, which suggest an extracellular agent, and results from the periphery that suggest an intravascular agent.

Because of these problems, we made the decision to switch to ferumoxytol (Feraheme) as our contrast agent. Unlike Ablavar, ferumoxytol is not an FDA approved contrast agent. Ferumoxytol is an iron-based compound that is clinically indicated for iron-replacement therapy in patients with chronic kidney disease. But because it is iron-based, ferumoxytol also has significant T_1 and T_2 shortening properties that make it suitable for use as MR contrast, and it has been previously studied as an agent to measure cerebral blood volume [64-66]. Because of its FDA approval status and history of research use to measure tissue blood volumes, ferumoxytol seemed ideally suited for measuring MBV. Unfortunately, after the experiments performed below had taken place, the FDA issued a black-box warning for ferumoxytol, which has thrown any further use of ferumoxytol into doubt. This is discussed further below in the discussion section of this chapter.

2.4: Methods

2.4.1 Image Acquisition

12 healthy volunteers were recruited for an MRI scan. 1 subject was excluded due to arrhythmia discovered during scanning, and 1 subject was excluded to due to injection error. In total, 10 subjects were analyzed in this study. All images were acquired with a 1.5T scanner (Siemens Medical Systems, Erlangen, Germany). Each volunteer was given multiple small boluses of ferumoxytol. Ferumoxytol was diluted 4x and subjects were given no more than 4mg/kg, as described in [64, 65]. Ferumoxytol was injected at 3ccs/sec, and during ferumoxytol injection each subject was imaged using a saturation recovery, Cartesian, TurboFLASH sequence (TR/TE

= 1.70/1.14 ms, saturation recovery time 110 ms, flip angle 12°, slice thickness 8 mm, in-plane resolution = 1.40 mm, acquisition matrix = 204x256). A single mid-ventricular slice was imaged. Before and after each injection, a MOLLI sequence (flip angle 35°, slice thickness 8mm, in-plane resolution 1.40 mm, acquisition matrix 218x256) was used to acquire T_1 mapping data at the same mid-ventricular slice location.

2.4.2 Phantom

Because MBV is calculated using ratios of relaxivity changes, obtaining accurate T_1 measurements is crucial to accurately measuring MBV. In this experiment we used a MOLLI sequence, which is a well known and widely available sequence for measuring T_1 in cardiac MRI. Bloch simulations have shown that short T_2 times can introduce error into MOLLI T_1 measurements[67], so we conducted a phantom experiment to verify that our MOLLI sequence was accurately measuring T_1 in spite of the strong T_2 relaxation properties of ferumoxytol. In the phantom study, we compared the above MOLLI sequence to an inversion recovery spin echo (IR-SE) sequence (TR=3000, TIs: [22 50 80 120 180 250 400 550 750 1000 1750 3000]). Serial dilutions of ferumoxytol were performed, yielding concentrations shown in **Table 1**, tubes containing the dilutions were suspended in a water bath, and they were imaged using the MOLLI and IR-SE sequences. The MOLLI sequence was repeated 27 times in order to estimate the precision of the sequence in this setting.

2.4.3 Image Analysis

T_1 and perfusion images were loaded into Medis QMass v6.5 (Medis medical imaging systems bv, Leiden, The Netherlands) for drawing epicardial contours, endocardial contours, and blood

pool regions of interest. Signal intensity (SI) data from six equiangular segments of the mid-ventricular short axis slice was extracted and averaged to generate SI curves for each AHA bullseye segment. All further analysis was performed in Matlab (The Mathworks Inc, Natick, United States).

T_1 values were calculated from MOLLI signal intensity data by using a three variable Look-Locker fit. Because it can be ambiguous whether points early in an inversion recovery curve represent positive or negative magnetization, multiple fits were done using different inversion time cutoffs for when the recovery curve passed through zero magnetization. The T_1 was then taken from the fitted curve with the least residual error **Figure 8**.

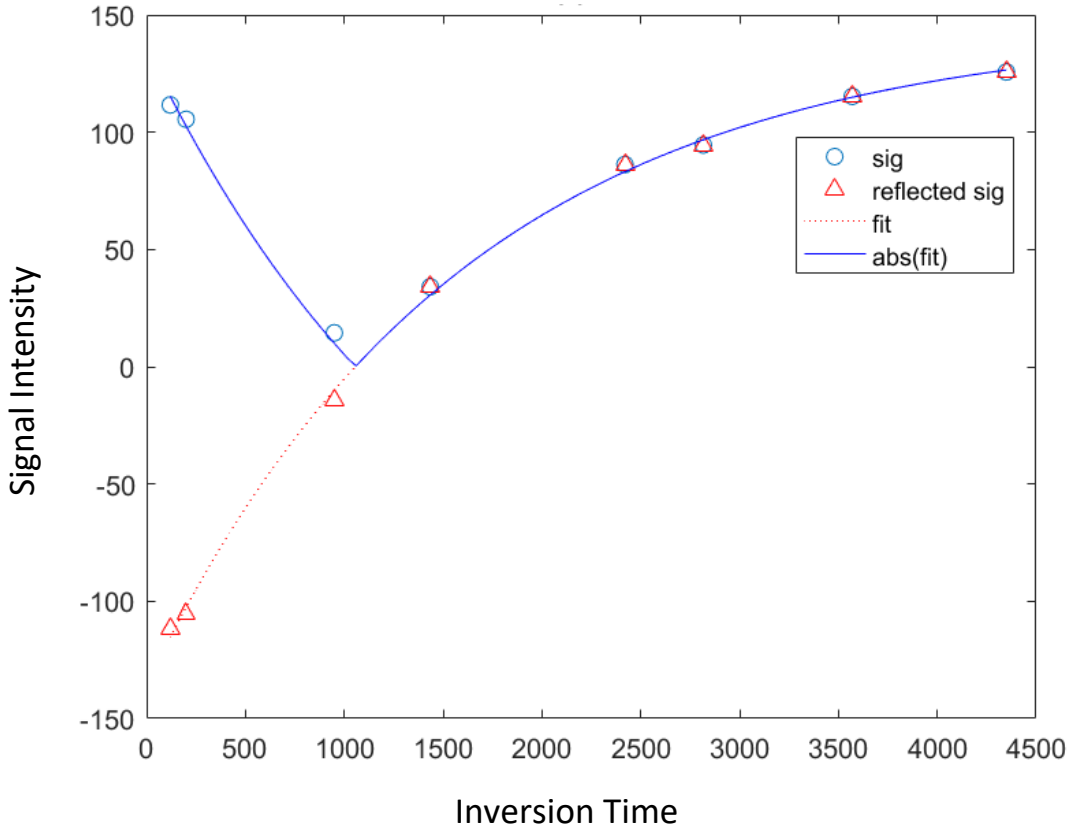

Figure 8: MOLLI fitting
The reflected signal is found empirically by selecting the number of reflected points that minimizes T_1 fitting error

2.4.4 MBV and Water Exchange Fitting

For each subject, after determining the myocardial and blood pool T_1 values after each contrast dose, the baseline pre-contrast T_1 values were subtracted to yield a series of ΔR_1^{blood} and ΔR_1^{myo} measurements. These values where then used to calculate an observed MBV uncorrected for water exchange as in Equation 13. The ΔR_1^{blood} and observed MBV were then used in the fitting model as described above in the Theory section in order to calculate a true MBV and exchange rate.

2.5: Results

The T_1 values as measured by IR-SE and MOLLI are shown in **Table 1**. The r_1 relaxivity constant calculated from the IR-SE measurements was 16.28, which is 8.5% larger than the value of 15 reported in the literature [68].

Table 1: Ferumoxytol phantom measurements
MOLLI T_1 values were both precise and consistent with gold-standard IR-SE measurements above a T_1 of 41ms

molarity	T_1 (IR-SE)	T_1 (MOLLI)	%difference	Standard deviation (as % of value)
2.28	27.1	39.3 ± 2.95	45.2	7.5%
1.43	40.8	41.5 ± 1.40	1.7	0.3%
0.46	143	129 ± 2.37	-10.1	1.9%
0.23	244	241 ± 1.38	-1.0	0.6%
0.13	413	415 ± 4.57	0.5	1.1%
0.09	607	619 ± 2.00	2.0	0.3%
0.05	894	917 ± 2.51	2.6	0.3%

For 8 subjects, all T_1 data were fit without issue. For 2 subjects, the blood pool became sufficiently saturated with contrast the T_1 values were too small to calculate a T_1 fit. Once a data point was unable to be fit, that data point and all subsequent data points for that subject were excluded from analysis.

The best fit MBV and exchange frequency simulations using the global myocardial average in each subject are plotted in **Figure 9**. The mean MBV was 10.0 ± .7% and the mean exchange frequency was 6.9 ± 2.4s^{-1}. These results are summarized in **Table 2**. MBVs calculated using

segmental instead of global averages are shown in **Table 3**. Of the myocardial segments, sectors 1 and 2 had MBVs significantly different than the myocardial average ($p<.05$).

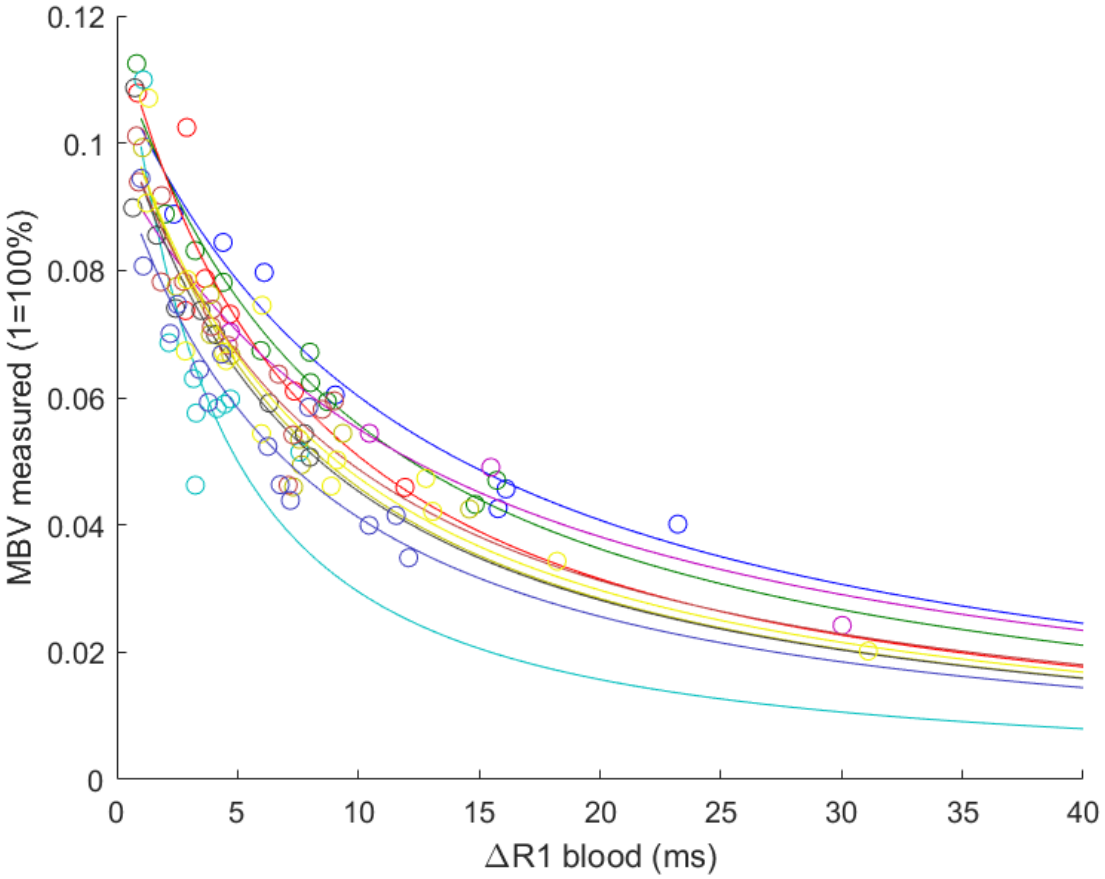

Figure 9: Measured MBV data and best fit simulations in volunteers
Circles represent experimental measurements and solid lines are best fit simulations

Table 2: MBV and exchange frequency fits in volunteer cohort

Subject	MBV (%)	1/tau (s^{-1})
1	10.5	9.8
2	10.7	7.8
3	11.0	6.0
4	10.7	2.3
5	9.2	11.3
6	10.0	6.0
7	9.7	6.2
8	9.7	7.3
9	10.0	6.5
10	8.9	6.2
mean	10.0 ± 0.7	6.9 ± 2.4

Table 3: MBV in volunteers organized by AHA segments

Segment	MBV (%)
S7	12.6 ± 2.8
S8	14.0 ± 5.2
S9	9.7 ± 1.9
S10	11.3 ± 1.8
S11	11.2 ± 1.9
S12	10.0 +/- 2.2

Comparing the measured MBV to the best fit true MBV allows for the calculation of measurement error for each MBV measurement (i.e. the error introduced by water exchange effects). The measurement error for all subjects is shown in **Figure 10** as a function of blood pool relaxivity change. An exponential fit of the form Y=A(1-exp(B*X)) + C was calculated using least squares minimization and used to derive a global correction curve and remove error from water exchange. We found the best fit of the error to be

$$\frac{MBV_{meas} - MBV_{true}}{MBV_{meas}} = -0.72\left(1 - e^{-0.16\Delta R_1^{LV}}\right) + 0.054 \quad (28)$$

Which from algebraic rearrangement results in a correction curve of

$$MBV_{est} = \frac{MBV_{meas}}{-0.72\left(1 - e^{-0.16\Delta R_1^{LV}}\right) + 1.054} \quad (29)$$

Where MBV_{est} is an estimate of the true MBV found by solving Equation 28 for MBV_{true}. This allows for calculation of an approximate true MBV using only a single datapoint instead of using the mathematical model on a series of datapoints as described above. The MBV estimate and error in this estimation is plotted in **Figure 11**

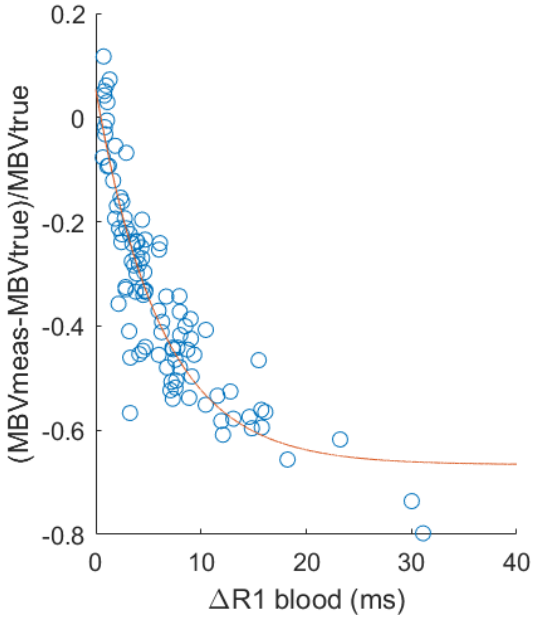

Figure 10 Error in measured MBV as a function of blood pool relaxivity change

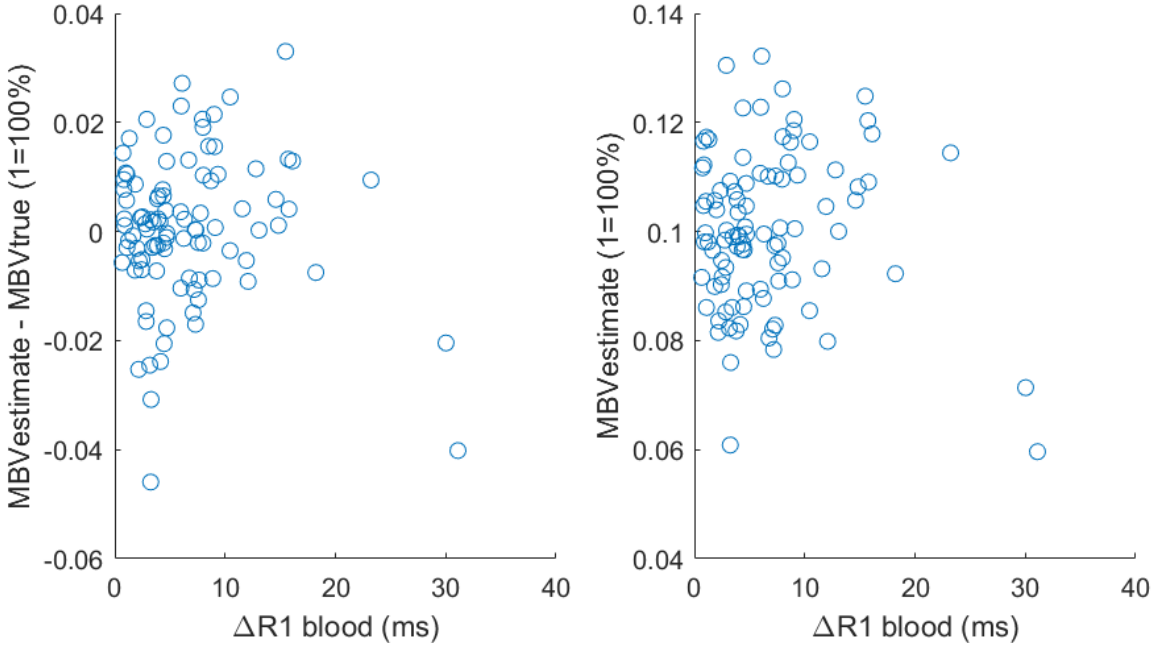

Figure 11: MBV estimates from single post-contrast T1 measurement.
Shows the difference between the estimated MBV using Equation 29 vs the best fit true MBV from fitting all datapoints

In the perfusion series, contrast passage was readily visible in the blood pool and myocardium for all subjects. Because the injection protocol in this study was focused on mapping MBV over a wide change in blood pool T_1 changes, the initial contrast injection in most subjects resulted in relatively small signal intensity changes. An example signal intensity curve for one of the subjects with a relatively higher initial T_1 change is shown in **Figure 12**.

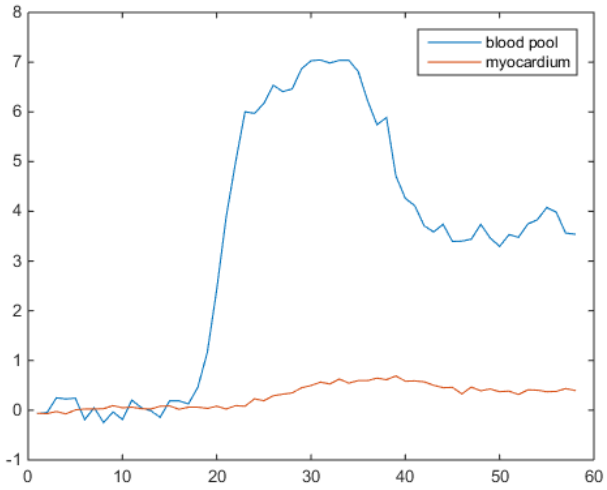

Figure 12: First pass signal intensity change from ferumoxytol bolus

2.6 Discussion

In this study, we investigated the use of an intravascular contrast agent to measure myocardial blood volume in a group of healthy volunteers. When using relative changes in relaxivity to calculate MBVs, we found that water exchange effects caused significant measurement error, which manifested as large variations in MBV that depended on the dosage of contrast agent used. However, when applying a fitting algorithm using the Hazlewood model, we found that the MBVs of all subjects fell within a tight range that is consistent with values seen in the literature. Furthermore, we found that the error introduced by water exchange effects was similar in all

subjects, which allowed us to construct a simple correction function to remove water exchange measurement errors. These results demonstrate the feasibility of using ferumoxytol to quantitatively measure myocardial blood volume.

While MBV is closely related to perfusion in terms of physiology, MBV has not been as well studied as perfusion. Still, MBV holds promise as a potentially important biomarker for cardiovascular disease. Research in animals has indicated that MBV may hold similar or complementary information to perfusion in the assessment of coronary artery disease (CAD)[56]. As such, MBV could potentially play a role as important adjunct to perfusion in the characterization of CAD in patient populations. Additionally, while perfusion is currently an excellent marker for focal disease such a single or double vessel coronary artery disease (CAD), it has a less clear role in global myocardial disease. The vast majority of perfusion scans only measure *relative* perfusion (e.g. visual inspection for dark areas or upslope ratios), not *quantitative* perfusion in ml/min/g. Because it is difficult to identify any global uniform defect with a relative metric, this makes it difficult to use perfusion to gain information about diseases that involve global microvascular dysfunction. However, because MBV is a quantitative metric, it may help in the identification of global disease processes. This is especially true when the disease has an effect on the microvasculature. Not only are such diseases generally global in nature, but microvascular disease could reasonably be expected to have an effect on the blood volume of the microvasculature. One such example of this type of disease process is cardiac allograft vasculopathy, which is a leading cause of death in heart transplant patients, and a recent study using contrast ultrasound[55] found diagnostic utility in MBV. MBV may be useful in other global disease processes, such as scleroderma, and development of an MRI protocol to

measure MBV in humans would facilitate more research and better understanding of these disease processes.

In spite of the great potential of MBV as a useful measurement, it is seldom studied and is not used clinically. One critical reason for this is that measuring MBV requires the use of an intravascular contrast agent, but almost all of the clinically used contrast agents are gadolinium agents that leak into the extracellular space. One important exception to this was gadofosveset (Ablavar), but as shown earlier gadofosveset does not behave as an intravascular agent during first-pass, so it would be impossible to gather both perfusion and MBV data in the same scan. There are several intravascular agents, however, and as demonstrated here with ferumoxytol an intravascular agent can be used to acquire both perfusion and blood volume data.

Even with an intravascular agent, another critical hurdle to measuring MBV is compensating for water exchange effects. Calculating a volume fraction from a simple ratio of relaxivity changes assumes that the voxel being measured is well mixed. While fast exchange may be a reasonable assumption between the extracellular and intracellular compartments as when calculating an ECV, the results of this study demonstrate that exchange between the intra- and extra-vascular compartments is slower, and that fast exchange is not a valid assumption for calculating MBV. This finding is illustrated in **Figure 10**, which shows the MBV measurement errors introduced by water exchange effects. As seen in the figure, measurement error increases with contrast dose and measured MBVs may be as much as 60% underestimated at higher doses. For MBV to be a useful and repeatable measurement, its measurement cannot be dependent on contrast dose given, so it is critical that these exchange effects are accounted for when calculating MBV.

Here we demonstrate a way using a Hazlewood two-compartment model to determine the water exchange rate and compensate for its effects. When applying the model to our cohort, we found that the MBVs tightly clustered around 10% and a mean exchange frequency of $6.9s^{-1}$. This is in agreement with animal models that have shown MBV values of 6-11% and exchange frequencies of 5-9 s^{-1}. While the exchange frequencies showed a fair amount of subject to subject variation, the MBV was surprisingly consistent between subjects. All but one subject had an MBV in the range of 9-11%. With a sample size of only 10 subjects, conclusions cannot yet be drawn to larger populations, but the tight clustering of MBV values observed here suggests that MBV is highly regulated and falls within a narrow range in healthy people. If true, this has the potential to be of great diagnostic utility as it would be easier to say with confidence that any MBV measured outside of this narrow range represents some sort of pathology. This is different than, for example, perfusion measurement where a typical resting perfusion study can show perfusion values ranging from 0.5 to 1.5 ml/min/g.

One of the aims of this study was to work towards an implementation of the Bookend technique for measuring myocardial perfusion, which is a method for measuring quantitative perfusion by using blood volume calibrations[47-51]. To this end, we sought to find a way to approximate the results of the Hazlewood model so that MBV could be measured using only a single pre- and post-contrast T_1 measurement. Fortunately, when we examined the error introduced by water exchange effects, we found that the error was well predicted by an exponential function of the blood pool relaxivity. This allowed us to construct a water correction function to correct any single measured MBV for water exchange effects without having to perform serial contrast boluses and T_1 measurements to map out an entire water exchange curve. When applied to the

data collected in this study, we found that most of the corrected MBVs fell within +/- 2% of the true MBV **Figure 11**. Additionally, when comparing **Figure 10** to **Figure 11**, it is readily apparent that while the measured MBVs show a systematic underestimation of the true MBV, the corrected MBV errors are centered around 0% and do not show a positive or negative bias. These results indicate that is feasible to correct for water exchange effects using a simple algebraic expression that relies on only a single pre-contrast and post-contrast measurement. This result is important for perfusion measurements because it removes the need for multiple bolus injections, instead allowing the use of a single large bolus. In this study, we found that contrast was readily visible on first pass, but as seen in **Figure 12** the myocardium signal change in a typical subject was small due to the small contrast injections. Replacing the multiple small boluses with a single larger bolus would result is higher quality perfusion data. However, more work is needed to adapt the Bookend technique to myocardial data and to compare ferumoxytol perfusion measurements against more typical measurements acquired with gadolinium contrast agents.

A limitation of this study is the absence of any subjects with known pathology. While having corrected MBVs fall within +/- 2% of the true MBV seems to represent a relatively small error in absolute terms, compared to the average MBV of 10% this represents a 20% error relative to a typical measurement. Without knowing how much MBV varies in pathological settings, we cannot say whether or not this in an acceptably low error rate for diagnostic use. Similarly, the segmental MBVs within each subject were close to the mean of the whole myocardium (**Table 3**) except for sectors 1 and 2, which showed a slight increase in MBV relative to the average MBV of the whole myocardium ($p<.05$). It is possible that this represents artifact from the septal

area, which moves throughout the cardiac cycle. However, Sectors 1 and 2 represent the left anterior descending (LAD) territory, so it is also possible that some subjects had LAD disease that they were unaware of. Without angiography, which was not performed in our volunteer cohort, we could not verify the absence of CAD and instead relied on subject self-report. A repetition of this experiment in a patient cohort with quantitative coronary angiography would help characterize the relationship between CAD and MBV, allow us to better understand the degree of accuracy and precision needed to identify pathology, and might help explain the segmental variations in MBV seen in this study.

The most important limitation of this study is the absence of a gold standard reference value to validate the MBV measurements. That the calculated MBVs according to our model show little variation and fall within expected physiological limits strongly suggests that the method presented here can calculate quantitative MBV values, comparison to a gold standard would provide more definitive proof. Gold standard measurement in animal models use gamma counting, but because this requires tissue samples it was not feasible to carry out in a study of myocardium in a volunteer cohort. This could perhaps be done in a patient cohort where MRI measurements of MBV can be compared to other modalities (e.g. contrast ultrasound) or where biopsy specimens are collected as part of clinical care, such as in post-transplant patients. However, even if this were possible, the absence of perfusion pressure in *ex vivo* samples could cause a collapse of the microvasculature, and there is no guarantee that *ex vivo* MBV measurements would be a true representation of *in vivo* MBV. Other potentially feasible methods for measuring MBV include contrast echocardiography or SPECT imaging with tagged

blood cells. However, neither of these were feasible to implement in this study of healthy volunteers.

Lastly, it should be noted that the contrast agent used in this study may not be acceptable for future use in MBV measurements. After the completion of the experiments described in this study, the FDA issued a "black box" warning about anaphylaxis risk in persons receiving intravenous ferumoxytol [69]. This warning was based on ferumoxytol's clinical use as an iron therapy agent in anemic patients with chronic kidney disease. With anaphylaxis as a potential risk of ferumoxytol administration, it may be hard to justify its use in any sort of routine diagnostic setting, instead limiting its use to patients where there is a clear potential benefit. However, there are many important caveats to this FDA warning that provide some hope that ferumoxytol may actually be safe to use as a contrast agent. First, this warning was based on patients receiving a clinical dose of 510mg infused at 1ml/s with another 510mg follow up dose 3-8 days later. This is far greater than the dose needed for imaging, which in this study was a *maximum* of 4mg/kg. For a 70kg individual, this represents less than 60% of the 510mg clinical dose. Second, because MBV is measured in steady state, ferumoxytol could be administered arbitrarily slowly, reducing the risk associated with a large bolus injection. Unfortunately, this would preclude the use of ferumoxytol for measuring perfusion. Lastly, this warning was based on patient use, which necessarily includes people that may be suffering from kidney, liver, or other disease. As noted in a recent review of ferumoxytol safety in MRI use, nearly a quarter of the patients that led to the boxed warning had multiple drug allergies and the rate of adverse events in postmarket surveillance is actually lower than the rates initially reported in phase II-III clinical trials[70]. It is possible that the anaphylaxis risk is only significant in populations

suffering from a particular disease and that ferumoxytol would be safe for use outside of this population. This would mirror the history of gadolinium contrast use, which for a time was thought to be potentially unsafe because of risk of nephrogenic systemic fibrosis (NSF) until it was discovered that NSF only occurred in individuals with impaired kidney function. In fact, a recent study has been published about ferumoxytol use as a contrast agent [71], and they report that they are unaware of any anaphylaxis cases with diagnostic use of ferumoxytol. Still, they ultimately recommend that its use be limited to setting where there is a strong clinical indication. In total, we believe that currently the risk is too great to continue using ferumoxytol in any sort of healthy volunteer research setting, but paradoxically without further research it is difficult to identify cases where there is a clear patient benefit. However, we are hopeful that future data will show ferumoxytol to be safe for use many applications. In the interim, there are other intravascular iron-oxide contrast agents that do not carry the same anaphylaxis risk as ferumoxytol. Water exchange is a physiologic process that should be dependent on tissue properties, and while we cannot say definitively without repeating these experiments, the results presented here should apply to other intravascular contrast agents as well.

In summary, we present a way for quantitatively measuring myocardial blood volume and water exchange frequency in humans using an intravascular contrast agent. We found that water exchange effects cause a significant underestimation of true blood volume when not accounted for. However, we also present two methods of compensating for water exchange: one by using multiple T_1 measurement to simulate water exchange, and one by using an algebraic approximation of the measurement error as a function of T_1 change. As techniques for accurately measuring myocardial blood volume become more widely available, myocardial

blood volume may develop into an important diagnostic metric for use in research and clinical environments.

Chapter 3: Dual Bolus Quantitative Perfusion and Empiric Tail Correction

3.1: Introduction

After the FDA issued a black box warning on ferumoxytol, we elected to investigate another route to implementing quantitative perfusion. As noted in the introductory chapter, MR perfusion imaging uses signal intensity over time as a surrogate for contrast concentration over time, but this assumes a linear relationship between MR signal and contrast concentration. Virtually all first-pass techniques suffer from saturation of the AIF signal during the peak of the contrast bolus, which results in underestimation of the AIF and errors in calculated flow. Several current methods have been proposed to measure an unsaturated AIF, but for various reasons none of them have seen much use, especially in clinical environments. One of the more well known methods is dual bolus, which addresses the problem of AIF signal saturation by using a low-dose contrast bolus to measure the AIF and a separate high-dose contrast bolus to ensure adequate myocardial signal. Content in this chapter includes text and figures reprinted from a publication currently in press.

While Dual Bolus can effectively solve the AIF saturation problem when performed correctly, in practice dual bolus is seldom used outside of a few academic centers in large part because it can be very difficult to implement. For any Dual Bolus experiment, two contrast agent mixtures of different contrast concentration but equal volume and identical delivery rate are needed: the "full" bolus used to measure signal in the myocardium and a more dilute "mini" bolus used to measure the AIF without saturation effects. There are several different proposed methods for implementing this sort of protocol, none of which have been adopted as a universal standard. One method of accommodating both bolus concentrations is to use a separate power injector for

each bolus. However, obtaining a second injector is costly, and most clinical MR scanners only have access to a single injector at a time. When a second injector is not available, a preloading scheme can be used[46]. Another single injector alternative has been proposed[72], but this requires the presence of a physician for a manual contrast push. While both of these avoid the cost of a second injector, they add time and complexity to the experimental setup, which is a significant hurdle in busy clinical environments where time is scarce and procedures are typically performed by MRI technicians and not dedicated cardiovascular MRI researchers. A typical clinical protocol also includes two perfusion studies (one at rest and one under stress), which would require preparation of separate lengths of tubes that are switched between the stress and rest studies. Existing microsphere validation of dual bolus has focused primarily on stress perfusion [44], and it is unclear what effect a more complicated stress/rest protocol would have on dual bolus accuracy and precision.

Not only is the experimental setup difficult for dual bolus, but care and attention to detail during this setup are crucial. In order to match the mini bolus AIF to the full bolus myocardial signal during blood flow calculations, the mini bolus AIF must be scaled by the ratio of contrast agent concentrations as measured at the left ventricle (LV). Accurate knowledge of this ratio is critical as even small errors in the ratio can cause significant changes in the resulting flow. Typically the mini bolus is created by diluting the full bolus, and the concentration ratio at the LV is assumed to be the same as the dilution ratio. However, creating the two mixtures will always involve some degree of experimental error, which will only be magnified when performed outside of tightly controlled research environments. An alternative method has been proposed by Köstler [45] that uses a summation of smaller volume (instead of lower concentration) pre-boluses.

While this technique does avoid dilution error, it is similarly susceptible to experimental error in that the summation is predicated on knowing a precise ratio of pre-bolus to full bolus volume. Finding an adjustment to the dual bolus technique so that it requires less careful setup and is more robust towards experimental error might facilitate more widespread adoption.

Fortunately, it should be possible to determine contrast concentration ratios empirically from the measured signal intensity data. Because only the peak of the AIF is saturated, the portion of the AIF after the signal peak should have minimal saturation effects. Thus, when scaled properly, the tail end of the mini bolus AIF and the full bolus AIF should match. If this information can be used to determine the contrast ratios empirically and reduce the effects of experimental error, it would both reduce scan-to-scan variability and make dual bolus easier to implement in less controlled environments. In this chapter, a tail matching method is presented for empirically deriving contrast concentration ratios in dual bolus experiments. We then investigated the effect of this technique on quantitative perfusion measurements and used the empirically derived contrast ratios to examine potential sources of error in dual bolus experiments. We hypothesized that empirically derived contrast ratios improve the quantification of myocardial perfusion when using a dual bolus scan protocol.

3.2: Methods

3.2.1 Simulations

Our motivation for this study is predicated on the idea that dual bolus perfusion measurements are highly susceptible to small changes in full to mini bolus contrast concentration ratios in the left ventricle. To investigate this effect, we took a representative AIF and myocardial signal

intensity data from an animal experiment (described below) and adjusted the contrast ratio from 8 to 12 in increments of 1 (true dilution ratio = 10). In each case, the myocardial flow was calculated as described below.

Our experimental determination of the contrast agent dilution ratio is derived from signal ratios acquired in the LV, after peak contrast enhancement in the "tail" of the bolus where saturation effects are negligible. To confirm the assumption that saturation effects are negligible in the tail of the AIF, we simulated the passage of full and mini bolus AIFs through the LV. The full bolus AIF contrast concentration was modeled using a gamma variate function[43, 73] in units of mmol/mL, and the mini bolus AIF was empirically derived by dividing the full bolus AIF concentrations by 10 (the dilution factor used in the experiments described below). Both AIFs, currently defined in terms of contrast concentration, were then converted to signal intensity using a baseline blood T1 of 1500ms (Field strength of 1.5T to match our experiments), the relaxivity of gadopentetate dimeglumine (Magnevist, Bayer Healthcare, Whippany, NJ) [74], and the SR-FLASH signal equation[5]. Simulations assumed a full bolus contrast concentration of 0.5mmol/mL, an injection rate of 4cc/sec, and a cardiac output of 5L/min. Additionally, to test the validity of the assumption that the scaled mini bolus is an approximately linear representation of the unsaturated full bolus, we also modeled the ideal case of an unsaturated full bolus signal. To model this ideal signal, the linear region of SR-FLASH signal equation[5] was extrapolated to higher contrast concentrations.

3.2.2 Animal Imaging

A total of 8 rest and 10 stress studies were conducted on 5 dogs in accordance with and after approval by our institution's animal care and use committee. Each animal was chronically

instrumented with an external hydraulic occluder and cuff-type Doppler flowmeter around the left circumflex or left anterior descending coronary artery as described previously[75]. Left atrial, right atrial, and aortic catheters were placed for the administration of fluorescent microspheres, phenylephrine, and withdrawal of reference blood samples, respectively. Animals that received more than one imaging study were allowed to recover at least 48 hours between studies. All stress perfusion studies were performed under maximal adenosine vasodilation. The adenosine infusion rate for each dog (140-420 mcg/kg/min) was that which produced the greatest increase in Doppler flow on a preliminary study. Except during reference blood withdrawals, the aortic catheter was used for continuous invasive blood pressure monitoring, and phenylephrine (40-80 mcg/min) was given to maintain mean arterial pressure > 60 mmHg. Different levels of coronary stenosis were achieved by varying the inflation level of the coronary occluder under Doppler flowmeter guidance for each study. During image acquisition ventilation was suspended to eliminate respiratory motion artifacts. The typical scan protocol was as follows: scouts, cine images, resting first-pass perfusion, stress first-pass perfusion. There was a minimum of 30 minutes between contrast injections.

All perfusion images were acquired with a 1.5T scanner (Siemens Medical Systems, Erlangen, Germany) with a saturation recovery, Cartesian, turboFLASH sequence (TR/TE = 2.21/1.39 ms, saturation recovery time = 100 ms, flip angle = 12°, slice thickness = 8 mm, in-plane resolution = 1.79 mm, acquisition matrix = 192 x 74). GRAPPA acceleration with an acceleration factor of 2 was used and no fat saturation was applied. Two or three short axis slices were scanned depending on the animal's heart rate at the time of imaging and the mid-ventricular slices were selected for further analysis.

Using a dual bolus protocol, two equal volume doses of gadopentetate dimeglumine (0.005 mmol/kg and 0.05 mmol/kg) were injected using separate power injectors (Medrad Inc., Indianola, PA) at a constant rate of 4 mL/s followed by a 12 mL saline flush injected at 4mL/s. The total volume in the lines between the saline syringe and the patient was 6.8 mL, and a schematic of the experimental setup is shown in **Figure 13**. Immediately following the high-dose contrast injection of each study, approximately $3x10^6$ microspheres (FluoSpheres Blood Flow Determination Color Kit #2, 15μm, invitrogen, Eugene, Oregon) were injected via catheter into the left atrium with simultaneous reference blood withdrawal from the aortic catheter. Microspheres with multiple unique fluorescence spectra enabled multiple imaging studies to be carried out in each animal.

After imaging, the animals were euthanized with an overdose of pentobarbital and each heart was fixed in formalin. 8mm slices corresponding to image acquisition slices were sectioned into six segments following the standard American Heart Association (AHA) bullseye segmentation[76]. Microsphere concentrations were quantified fluorometrically[77].

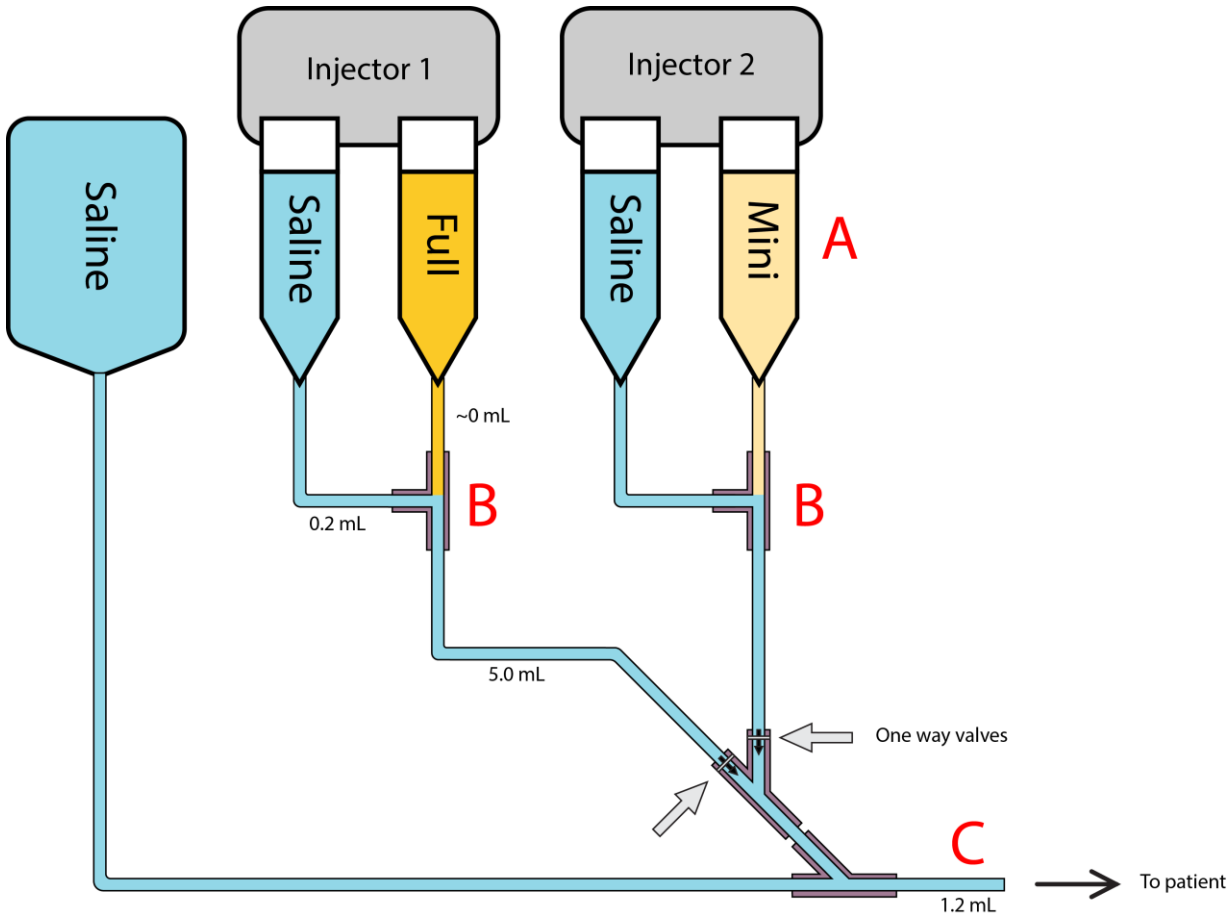

Figure 13: Schematic representations of dual injector setup for dual bolus perfusion. For this study, we used specialized Y-connectors with one-way valves to prevent backflow into the mini and full bolus lines. Volumes of the different components are shown (Y-connector = 0.4 mL). Potential sources of dilution error include (A) improper dilution of mini-bolus, (B) inadvertent mixing of saline and gadolinium, and (C) retention of residual contrast agent from prior bolus in IV line.

3.2.3 Patient Studies

Clinical records were queried to retrospectively identify patients who underwent clinically indicated adenosine stress first-pass myocardial perfusion imaging where a dual bolus injection scheme was utilized. 6 patients with quantitative coronary angiography (QCA) showing <30% stenosis in each of the major coronary vessels were used in this study. Adenosine was infused at

140 mcg/kg/min. After a minimum of 2 minutes infusion, equal volumes of Gd-DTPA (mini bolus 0.0075 mmol/kg, full bolus 0.075 mmol/kg) were injected using separate power injectors at a constant rate of 4 mL/s followed by 20 ml saline flush injected at 4 mL/s. The materials and design used for the dual bolus experimental setup were identical to those used in the animal study. However, scanning in the patient cohort was performed by MRI technicians during the course of normal clinical workflow whereas in the animal study all scanning was performed by MRI research personnel. Additionally, stress scans were performed first in the patient cohort but second in the animal cohort. Adenosine infusion was stopped after completion of the first pass of contrast through the left ventricle. After a minimum of 10 minutes, rest perfusion imaging was performed using the identical imaging and contrast injection scheme as stress perfusion imaging. Perfusion images were acquired with a saturation recovery, TurboFLASH sequence (TR/TE = 1.85/1.03 ms, saturation recovery time = 105 ms, flip angle = 12°, slice thickness = 10 mm, in-plane resolution = 2.375 mm, acquisition matrix = 160 x 120) on a 1.5T scanner (Siemens Medical Systems, Erlangen, Germany). Images were analyzed identically as in the animal study.

3.2.4 Image Analysis

Images were loaded into Medis QMass v6.5 (Medis medical imaging systems bv, Leiden, The Netherlands) for drawing epicardial contours, endocardial contours, and blood pool regions of interest. Signal intensity (SI) data from six equiangular segments of the mid-ventricular short axis slice was extracted and averaged to generate SI curves for each AHA bullseye segment. All further analysis was performed in Matlab (The Mathworks Inc, Natick, United States). A time offset was added manually to each mini bolus to ensure temporal alignment with the corresponding full bolus. SI in each segment was normalized using the mean of the first ten time

points prior to contrast arrival and the normalized baseline was then subtracted. Dual bolus correction was performed (see below for further details), and a Tofts-Key two-compartment model that includes fitting of the blood plasma volume[41] was used to calculate K^{trans} for each segment from the normalized ΔSI data. Blood flow was then calculated from K^{trans} using extraction fractions[78]. An extraction fraction of 0.46 was assumed for regions with MBF less than or equal to 2.9 ml/min/g and 0.32 for higher MBF regions. K^{trans} is known to vary with blood flow, and this cutoff was chosen as a rough approximation of the results in [42].

3.2.5 Dual Bolus correction

After SI normalization, SI data from the mini bolus AIF was temporally shifted so that the arrival times of the AIF (determined visually) were identical for the full and mini bolus. The SI data for the mini bolus was then interpolated using a piecewise cubic spline interpolation to match the acquisition times of the full bolus AIF. Two separate scalings of the mini AIF were then done, generating two different AIF curves. One was done using an assumed ratio of 10:1 for contrast concentrations in the full:mini boluses. The other was scaled using an empirically determined concentration ratio.

To empirically derive the contrast concentration ratio, we scaled the mini bolus SI curve such that the SI data at the tail end of the scaled AIF best overlapped with the full bolus AIF. To find the optimal matching, the tail was defined in each case as a relatively steady state period towards the end of signal acquisition. The second pass peak was avoided in order to minimize any potential saturation effects. In this region, SI data should be mostly unsaturated, so when scaled correctly the mini bolus SI curve should overlap the full bolus SI curve. To achieve maximum

overlap, least-squares fitting was used to find the full:mini ratio that minimized the difference between the two SI curves in this region (Figure 3b).

3.3: Results

3.3.1 Simulation

The newly scaled AIFs and resulting perfusion calculations are shown in **Figure 14**. Using the assumed dilution ratio of 10, the resulting flow was 2.6 ml/min/g. Adjusting the assumed ratio to 8 caused the calculated perfusion to increase 30% to 3.3 ml/min/g. Adjusting the assumed ratio to 12 caused the calculated perfusion to decrease 17% to 2.1 ml/min/g.

For the saturation simulation, simulated signal intensity curves are shown in **Figure 15**a. As expected, due to saturation effects on the full bolus, the peak of the scaled mini bolus is much larger than the peak of the full bolus (84% larger). However, in the indicated segment of the tail, the mini bolus signal intensity was only 5.1% larger. When comparing the scaled mini bolus to the ideal unsaturated signal, the peak of the scaled mini bolus was 96% of the height of the unsaturated peak.

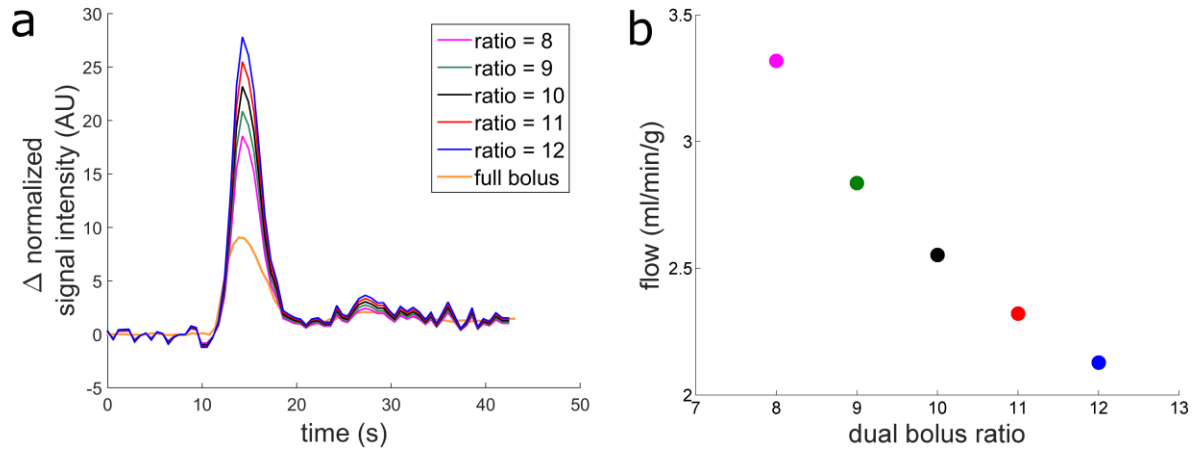

Figure 14: AIF and flow variability as a function of contrast concentration ratios.
a) A variety of scaled mini bolus AIFs are plotted assuming different full:mini contrast ratios. b) Mean perfusion in a segment of the mid-ventricular slice using each AIF. As the assumed contrast ratio decreases, the AIF peak falls and the resulting calculated myocardial perfusion is higher.

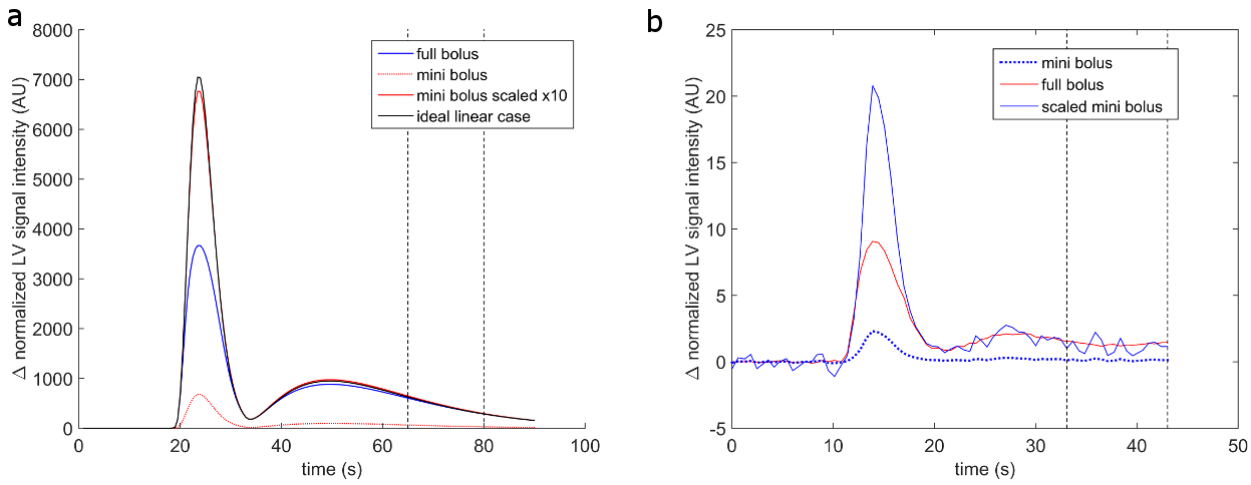

Figure 15: Empiric Tail Correction of Dual Bolus
a) Simulation of signal intensities from passage of full and mini boluses through the left ventricle. Saturation effects are apparent during the peak of the mini bolus but are small (5%) in the indicated portion of the tail. b) Example AIF calculated using tail-matching. The original mini bolus (dotted line) is scaled to minimize the difference between the mini and full boluses in the region between 33 s and 43 s post injection). While the assumed contrast ratio is 10:1, the empirically derived contrast concentration ratio is 9.0:1. Because there is minimal saturation of the MR signal in this region, when scaled correctly the mini bolus overlaps with the full bolus in this region.

3.3.2 Animal Study

108 mid-ventricular myocardial segments were analyzed. Using an assumed contrast concentration ratio of 10:1, the correlation coefficient of MR perfusion with microspheres was .84 with a slope of .62. Using the tail-corrected empirically derived contrast ratios, the correlation coefficient was .90 with a slope of .82 (**Figure 16**). The correlation coefficients were compared as described by Zou et al [79] using an R implementation [80]. The 95% confidence interval for the difference between these coefficients is [.035, .102], indicating that the difference is statistically significant. Additionally, the slope of the best fit linear regression relating MR perfusion to microsphere perfusion changed from .62 to .82 with 95% confidence intervals of [.54 .69] and [.74 .89]. These confidence intervals do not overlap, which demonstrates that the ratio of MR perfusion to microsphere perfusion is significantly closer to 1:1 when using the empirically derived contrast ratios. Without empiric correction, the correlation between K^{trans} and microsphere was .85 with a best fit slope of .24. With empiric correction, the correlation coefficient was .89 with best fit slope of .30 (**Figure 16**). Both the correlation coefficient and best fit slope changes were significant at $p<.05$.

The mean tail-corrected empirically derived contrast concentration ratio was 8.51 ± 1.53. This was significantly different than the assumed dilution ratio of 10 ($p<0.001$). The mean empirically derived contrast concentration ratio was 9.40 ± 1.52 at rest and 7.78 ± 1.15 at stress. The rest empirically derived contrast ratio was not significantly different than the assumed dilution ratio ($p=0.27$) while the stress contrast ratio was significantly lower ($p<0.001$). The difference in contrast ratios between the rest and stress scans was significant ($p<.05$).

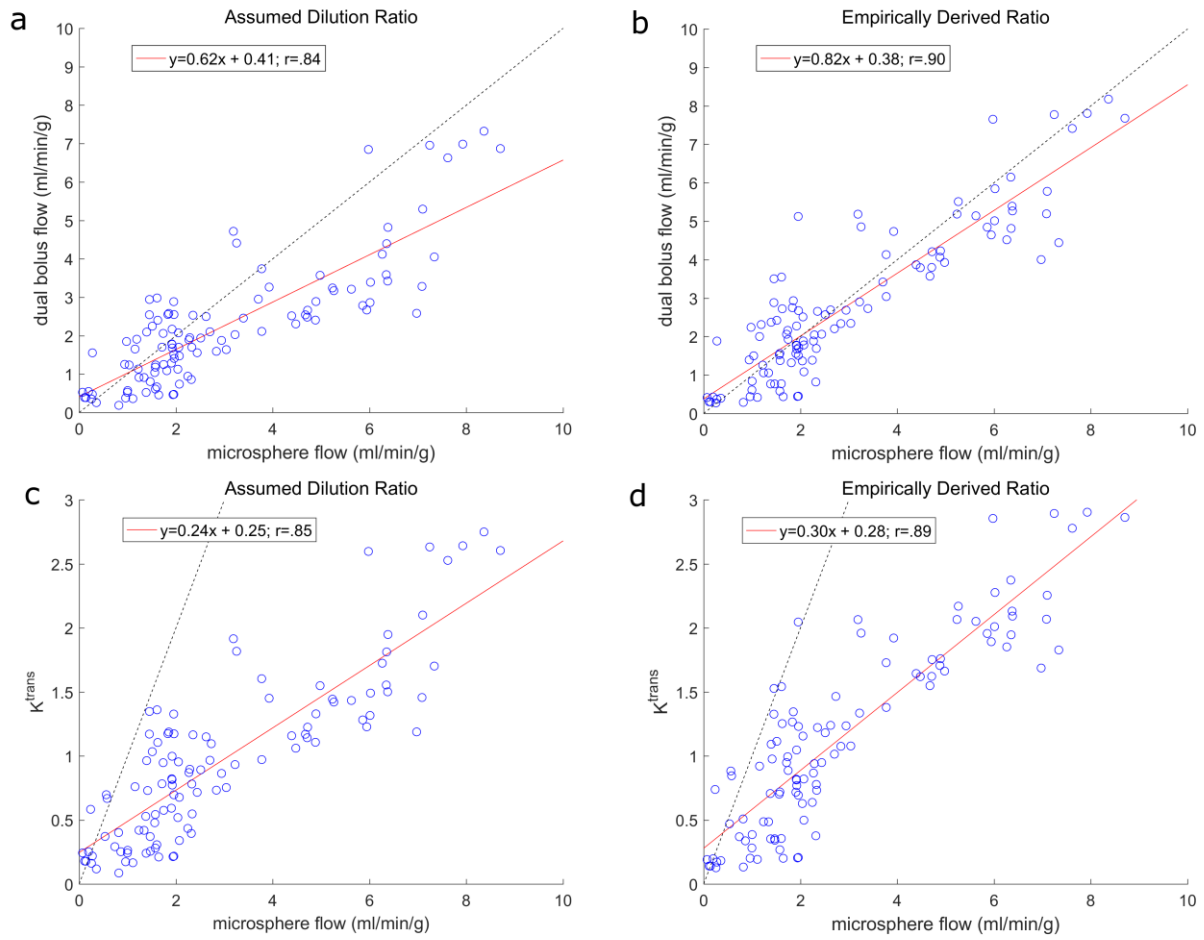

Figure 16: Myocardial blood flow in dogs before and after contrast ratio correction. Myocardial blood flow and Ktrans was calculated using both an assumed dilution ratio (a,c) and empirically calculated contrast ratios (b,d). Each plot includes both stress and rest data, and each datapoint represents the mean flow/Ktrans in a single mid-ventricular segment. Use of empirically calculated ratios improved correlation with gold standard microsphere measurements.

3.3.3 Human Study

The stress and rest flows, empirically derived contrast ratios, and flow reserves are summarized in **Table 4**. An example AIF is shown in **Figure 17**. The empirically derived contrast ratios were significantly different than the assumed dilution ratio ($p<.01$), however the difference in contrast ratios between the rest and stress scans was not significant ($p=.23$).

Table 4: Dual bolus perfusion measurements from patient cohort
Perfusion measurements from patient studies using both the assumed dilution contrast concentration ratio and empirically derived contrast ratio for perfusion calculation. *indicates difference of p<.05, **p<.01

	Empirically Derived ratio	Assumed Dilution ratio
Stress: Contrast ratio	4.79 ± 0.45**	10
MRI calculated myocardial blood flow (ml/min/g)	2.95 ± 0.67**	1.37 ± 0.28
Rest: Contrast ratio	6.56 ± 2.98*	10
MRI calculated myocardial blood flow (ml/min/g)	1.65 ± 0.20*	1.06 ± 0.40
Myocardial perfusion reserve	1.86 ± 0.53	1.59 ± 1.07

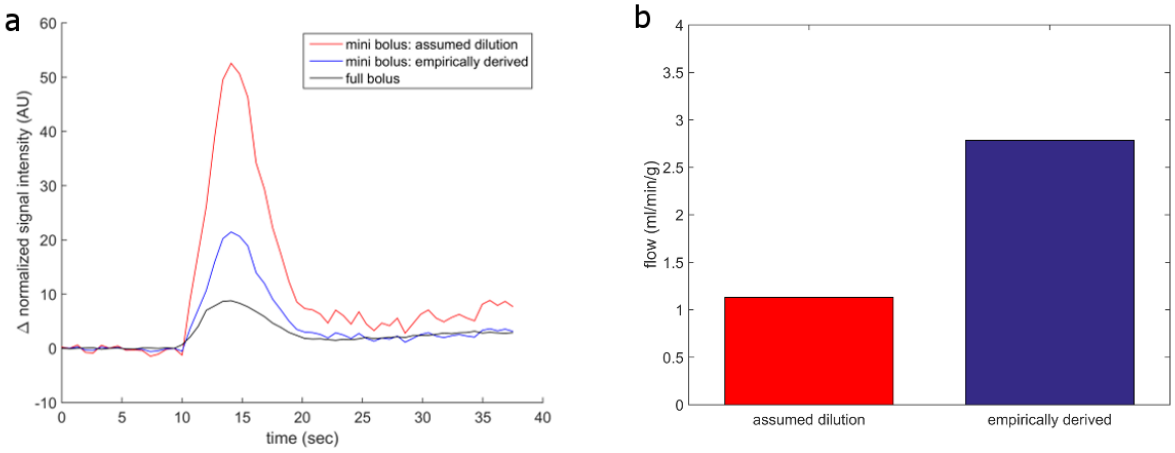

Figure 17: Empiric correction in a sample patient AIF
(a) Example patient AIF, before and after correction. Using the dilution ratio, the tail of the scaled mini bolus is much greater than the full bolus, and full bolus appears to be extremely saturated. When matching the tails (dashed segments), the full bolus appears less saturated, and the calculated flow is in a more normal physiologic range. (b) Mean adenosine vasodilated myocardial blood flow calculated using assumed dilution contrast ratios and empirically derived contrast ratios.

3.4: Discussion

In this study, we investigated the effect of contrast concentration ratio variability in dual bolus MR perfusion studies. Simulations confirmed the assumption that there are minimal saturation effects after the AIF peak, and we used this feature to find the empirically derived contrast concentration ratio that best matched the mini bolus to the unsaturated portion of the full bolus. When perfusion values calculated using the empirically derived ratios were compared to perfusion values calculated using the assumed dilution ratio, using the empirically derived ratio significantly improved correlation and agreement with gold-standard microsphere measurements. Furthermore, analysis of empirically derived ratios suggested that the actual ratios were on average 15% smaller than the assumed dilution ratio. These results indicate variation in contrast concentration ratios is an important source of noise in dual bolus perfusion measurements and that this variability can be mitigated by using ratios empirically derived from the AIF tails.

Dual bolus has been shown to be accurate in an ideal setting[44], but despite the advantages of having quantitative perfusion data, dual bolus adoption has been limited in scope. A major reason for this lack of adoption is that dual bolus experiments are difficult to perform in a routine clinical setting. Setup either requires a lengthy and complex preloading scheme or use of two power injectors[44, 46, 72]. Compounding this high degree of complexity in preparation is a low tolerance for experimental error as any change in contrast ratios has a large effect on final perfusion calculations. For example, suppose a typical experiment involves diluting 5mL of Gd contrast with 45mL of saline. An error of just 1mL in drawing up the Gd contrast will produce a 20% error in the mini bolus contrast concentration. As seen in **Figure 14**, this could introduce as much as 30% error into the final perfusion measurements, effectively negating any advantage of

absolute quantitative analysis. This type of error is easily conceivable if, for example, a single 50mL syringe is used to draw up both the Gd and the saline rather than using a separate 5mL syringe to more precisely draw up the Gd. The error potentially introduced by the sensitivity of this technique to what may seem like minor experimental details may help to explain why some studies have not found a significant advantage in using pre-bolus[81] or dual-bolus [82] over single bolus.

Reducing the experimental burden of using dual bolus may help both to increase its adoption and improve its accuracy. Some work has already been done in this area. Somewhat recently, a more universal method for performing dual bolus experiments was proposed[72], but it requires a physician for manual contrast push of the mini bolus. However, the vast majority of clinical MRI scans are performed by MRI technicians, and necessitating a physician present for scans adds a logistical burden that may not be feasible in many clinical environments. Additionally, adding another variable in the rate at which the mini bolus is pushed may further introduce variability between scans. Rather than focusing on modifying the dual bolus technique, we have instead focused on trying to improve the robustness of analysis to experimental error. Not only does this remove some complexity at the time of experiment, but it can also be applied retrospectively to existing dual bolus perfusion data.

In this study, we took advantage of the unsaturated regions of the AIF to empirically derive contrast concentration ratios at the left ventricle (**Figure 15**). First, this eliminates the need to know the dilution ratio, which makes this analysis tolerant of any experimental error in mixing the mini bolus. Second, what matters in the dual bolus experiment is not the contrast ratio at the injection site but at the site of AIF measurement, i.e. the left ventricle. So even in the case of a

perfectly precisely diluted mini bolus, the contrast ratio in the LV can be affected by changes in cardiac output, infusion rate (relevant for any bolus pushed by hand, as in [72]), or residual blood contrast. Because our method determines contrast ratios from LV data, much of this variability should be incorporated into the empiric ratio. As such, this method would be expected to reduce variability and improve accuracy even in tightly controlled experimental settings.

In our animal data, we found that using empiric ratios significantly improved dual bolus MRI perfusion against gold standard microspheres, indicating that our method was successful in reducing measurement error. When applying the same technique to real world patient data, we found that empiric ratios were significantly lower than the assumed dilution ratios. Accordingly, absolute perfusion values increased when applying the empiric correction. Not only did the absolute perfusion values fall into more expected ranges for a cohort without significant coronary vessel disease, but the standard deviation of the perfusion reserve decreased by over 50%. This indicates that using empiric ratios may increase the accuracy and precision of perfusion reserve measurements. A follow up study using a gold-standard (e.g. PET) comparison would better elucidate the accuracy of this method in real-world patient settings.

In both datasets, we found there was considerable variability in the empiric ratios. Reflecting the fact that the patient data was acquired in a less controlled setting, we found that empiric ratios in the clinical perfusion study deviated further from the dilution ratio. This indicates that in real-world data, assuming a contrast concentration ratio equal to the dilution ratio may introduce significant error into perfusion measurements.

While the tail matching technique to calculate empiric contrast ratios appears to reduce a significant source of error in dual bolus experiments, there are some important limitations to this

study. First, since we did not directly measure the contrast concentrations in the left ventricle, we cannot directly validate the accuracy of our contrast concentration ratios. Instead, we can only infer that they are more accurate than the assumed ratios based on how they affect perfusion measurements. It is likely that the empiric ratios include some degree of inaccuracy. The ratios are calculated from data towards the end of the scan, which is more likely to include respiratory motion. Also, as can be seen in Figure 3b, there is noise in tail, especially in the mini bolus as it is scaled from low signal intensities. We used a broad time period to reduce noise by averaging, but still some error is bound to remain. However, the fact that the empiric ratios improved perfusion measurements against gold standard microsphere data indicates that any error introduced by the empiric approach is less than the error it reduces.

Second, we cannot determine from this study the source of variability and/or inaccuracy in the contrast ratios. Changes in cardiac output or injection kinetics, experimental error, contrast leakage or residual contrast may all play a role in changing the real contrast ratio away from the dilution ratio, and without more experimentation we cannot say what role each factor plays. Despite efforts to limit error, Figure 1 illustrates several potential sites of error in our injection set up: (A) dilution error – any errors in measuring contrast, saline, or improper mixing will lead to actual dilution ratios that differ from the assumed 1/10 dilution; (B) leakage of contrast at saline/contrast T-junction – we used a specialized Y connector with one-way valves to prevent communication between the full strength and mini bolus contrast injector systems (Injector 1, 2). However, we used commercial injector kits, which do not include one-way valves at the T-junctions between contrast and saline injection syringes; (C) residual contrast in IV line – despite the use of adequate flush, some residual contrast remains in the IV line between the Y connector

and the patient after each contrast injection. One trend we did see in our animal data was that the contrast ratios during the first (rest) perfusion injection were not significantly different than the dilution ratios, but the ratios during the second (stress) perfusion injection were 22% smaller ($p<.001$) than expected from the dilution ratio. Importantly, existing microsphere validation of dual bolus used only a single stress scan, so it is unclear what effect a stress/rest protocol has on perfusion accuracy. Some preliminary phantom experimentation suggests that residual contrast from the first full bolus remaining in the IV line may have played a role in this finding, but without more testing it is impossible to state this with certainty. In the patient cohort we saw a similar trend of smaller stress than rest contrast ratios, although the difference was not significant ($p=.23$). In this case, residual contrast would not explain the difference as the stress scan precedes the rest scan in the patient cohort. It may be possible that other factors, such as leakage or dilution error, played a larger role in the clinical workflow, but at this point we cannot be certain what the underlying causes are. Ultimately, the causes of contrast ratio variability are multifactorial in nature. Some sources of variability may be systematic while others sporadic (i.e. human error), and sources of variability in one particular workflow or patient scan may be wholly different than those in another. While it may be of interest to determine the relative contributions to contrast ratio error in various settings, in practice it is likely more feasible to compensate for this error via a method such as the one presented here than to try to eliminate it entirely.

Lastly, an important limitation of all dual bolus experiments, including this study, is the assumption of a constant scaling factor. When applying the empiric contrast ratio to scale the mini bolus, we are implicitly making the assumption that the entire mini bolus can be scaled by

the same ratio. First, this implies that the dispersion of the two boluses is identical, and any change in cardiac output between the full and mini bolus may alter this. Also, the purpose of the mini bolus is to avoid signal non-linearity, and as seen in **Figure 15**, it is possible that the mini bolus peak exhibits some non-linearity. In an ideal case, this region would be scaled differently than the rest of the AIF. However, this would require knowing the degree of non-linearity at the peak, which differs based on contrast dose, hemodynamics, and sequence parameters. In practice, it is impractical to determine the degree of non-linearity, and instead a constant scaling factor is assumed for the entire AIF. As seen in Figure 2, the peak of the mini-bolus is typically similar to that of the ideal linear case, and assuming a linear response is fairly reasonable.

When considering these limitations, it is important to keep alternative methods for quantification in mind. While dual bolus is an imperfect method, there is no perfect method for myocardial perfusion quantification. Dual sequence[46] offers a conceptually similar approach to dual bolus, but it is susceptible to T_2^* effects and adds time to each slice acquisition, which may reduce spatial coverage. A single low dose can be used to minimize non-linearity, but this comes at the expense of losing signal to noise ratio (SNR) in the myocardium. Another method, constrained alternating minimization with model (CAMM)[83], uses an iterative series of constrained fits to derive an AIF, but this approach has yet to be validated outside of animal models. Each method for quantification has its advantages and disadvantages, including dual bolus. One of the principle disadvantages of dual bolus is its experimental complexity, and a central aim of our proposed method is to reduce the impact of any experimental error.

In summary, we have demonstrated a method for improving the accuracy of dual bolus MRI perfusion experiments by empirically determining left ventricular contrast concentration ratios

between the full and mini boluses. This reduces variability due to sources such as physiological noise and increases the tolerance of the technique to experimental error while acquiring data. In a real-world clinical environment, some degree of experimental error is inevitable. Increasing the robustness of analysis techniques eases the logistical burden on clinical staff and may help to promote a more widespread adoption of dual bolus myocardial perfusion MRI.

Chapter 4: Dual Echo Quantitative Perfusion

4.1: Introduction

With the experiments described in the previous chapter, we now had a workable method of obtaining quantitative myocardial perfusion data in a clinical environment. However, even having removed a significant degree of the experimental complexity associated with dual bolus, dual bolus remains in some aspects a non-ideal solution.

The first remaining problem with dual bolus perfusion is the remaining logistical complexity. In the previous chapter, we described a way for accounting for some of the effects associated with experimental error and in doing so removed some of the logistical requirements of having a precise setup. However, even with these advancements, dual bolus remains prohibitively logistically difficult to implement in many environments. The setup used at our institution for dual-bolus requires the use of a second contrast injector. Contrast injectors are non-trivially expensive, so requiring a second one adds significant cost that many institutions do not wish to or are not capable of covering. Dual bolus is possible with a single injector, but this comes with significant extra setup[72] required which can be difficult to justify in clinical environments where resources are limited and throughput is critical. An ideal quantitative perfusion method for use in a clinical environment is one that requires little to no extra setup by clinical staff and can be implemented very simply.

The second remaining problem with dual bolus is that, even when performed perfectly, there are confounders that are near impossible to control. The underlying assumption of dual bolus is that the “mini” and “full” AIFs are identical and that the *only* difference between them is the concentration of contrast in the bolus. For the kinetics of the AIFs to be the same, the injected

bolus must be of exactly the same shape and must be dispersed in exactly the same way as it travels from the injection site to the left ventricle. The first requirement, that the input bolus is identical except for concentration, is fairly well satisfied with the use of power injectors although would not be satisfied in setups (as in [72]) that substitute a manual contrast push for a second injector. The second requirement, that the input bolus dispersion is identical, is almost never truly satisfied and is only approximately true. This is because dispersion is a complex phenomenon that is dependent on several factors including cardiac output and vascular resistance. In some cases the dispersion is very similar, but in other cases it is not, but to a large extent this is outside of the control of the person performing the scan. An ideal quantitative perfusion sequence would not be so dependent on uncontrollable physiologic confounders.

Fortunately there is an existing quantitative perfusion method that, theoretically, circumvents both of these issues. Duel echo (also known as dual sequence) is a quantitative perfusion method that uses a separate image acquisition to acquire AIF data in a way that makes it less susceptible to non-linearity[46]. It requires no extra setup, only a modification of the pulse sequence used to capture the first-pass data. Additionally, it has many theoretical advantages over dual-bolus in terms of accuracy. However, in spite of these theoretical advantages, it remains infrequently used.

This lack of widespread adoption may be explained in part because dual echo data can be deceptive difficult to process. Like dual bolus, dual echo uses a smaller but unsaturated AIF as a surrogate for a larger saturated AIF. And like with dual bolus, there is a need to scale up the smaller unsaturated AIF to match the myocardial signal intensity data. To our knowledge, no method to do this has yet to be published in the literature. The original paper describing dual

echo does not describe any AIF scaling [46]. Without knowing this scaling factor, it is impossible to calculate absolute perfusion, only relative metrics such as a myocardial perfusion reserve (MPR) (defined as the ratio of flow at stress to rest) where the scaling factor cancels out. This may explain why the original paper only reported MPR values and not absolute perfusion at stress and rest. Additionally, to our knowledge, dual echo has only ever been validated against other MRI methods of quantifying perfusion (namely dual-bolus) and has never been directly validated against gold-standard measurements in an animal model.

Here, we present an adaptation of the empiric dual bolus scaling method applied to dual echo data. We then validate absolute perfusion values against gold-standard microsphere data in an animal model.

4.2: Dual Echo Principles

As discussed in Chapter 1, signal vs R_1 for an SR-TurboFLASH equation becomes increasingly non-linear as R1 increases (Figure 5). The degree of non-linearity observed is governed in large part by the time from the saturation pulse to image acquisition (TD). Figure 18 shows two different intensity vs R_1 curves, one for TD = 5ms and for TD = 85ms. As seen in the figure, the shorter TD sequence has a much more linear response but at the expense of signal intensity magnitude. Lowering the TD then represents a way to increase linearity at the expense of SNR. To make for an easier comparison to the other sequences described in this dissertation, dual echo is described here as a SR-TurboFLASH sequence, but the same principle applies to other sequences types as well such as GRE-EPI.

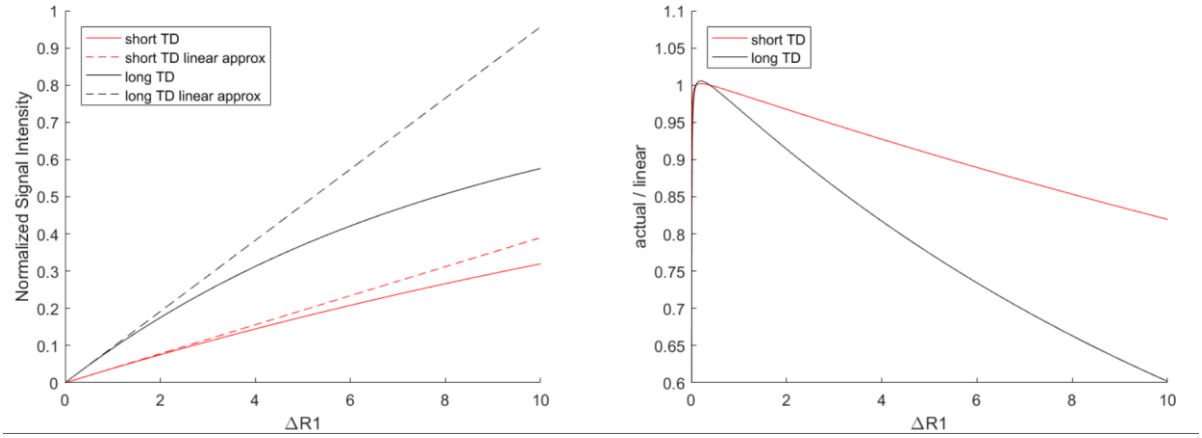

Figure 18: Signal linearity vs TD
Short TD sequences are more linear over a larger range of R_1 values at the expense of lower signal strength

Dual echo takes advantage of this tradeoff by using a short TD acquisition to measure the AIF (Figure 19). Because the short TD image is only used to acquire the AIF, it can be acquired quickly at low resolution. This short acquisition is beneficial because a short TD necessitates imaging in systole, during which there is much greater motion.

Similar to how the mini bolus AIF is combined with the full bolus myocardial data in a dual bolus experiment, in dual echo the short TD AIF is then combined with the myocardial data from the long TD acquisition. However, combining these two datasets is deceptively non-trivial. When calculating flow, signal intensity is used as a proxy for contrast concentration. Because R_1 (and thus contrast concentration) vs intensity is different for the AIF and myocardium they cannot simply be combined with no modification. Doing so would result an AIF that is the correct shape but drastically lower in amplitude due to the low SNR of the short TD sequence.

This would then result in a drastic underestimation of the contrast concentration in the AIF and consequent overestimation of perfusion.

There are two principle ways of trying to combine this data. One is to convert all the signal intensity values into contrast concentration values, at which point the AIF and myocardial data would both be measured in the same terms and could be combined. This could be done either by using T1 vs signal lookup tables for the short TD and long TD experiments or by comparing to a proton density weighted (PDW) image and solving for T_1 by using the SR-TurboFLASH signal equation. Both options have their drawbacks, including making assumptions about parameters, uniformity, and introduction of noise.

The other way to combine the data is to scale up the short TD AIF so that signal intensity vs contrast is the same for both the AIF and myocardium. If that can be done, signal intensity can again be used as a proxy and there is no need to convert to units of contrast concentration. In effect, this can be thought of multiplying the dashed red line in Figure 18a so that is equals the dashed black line in Figure 18a. In theory this scaling factor could be determined by the sequence parameters of the short TD and long TD sequences, but in practice this is difficult and changes from sequence to sequence.

Here we present a simpler alternative to scaling the short TD data that can be applied to any dual echo sequence. Similar in concept to the dual bolus correction, when the short TD AIF is scaled to have the same signal intensity vs R_1 as the long TD AIF the unsaturated parts of the AIF should be equal. We can use this property to empirically scale the short TD dual echo AIF to minimize difference between the short TD and long TD AIF in the unsaturated region.

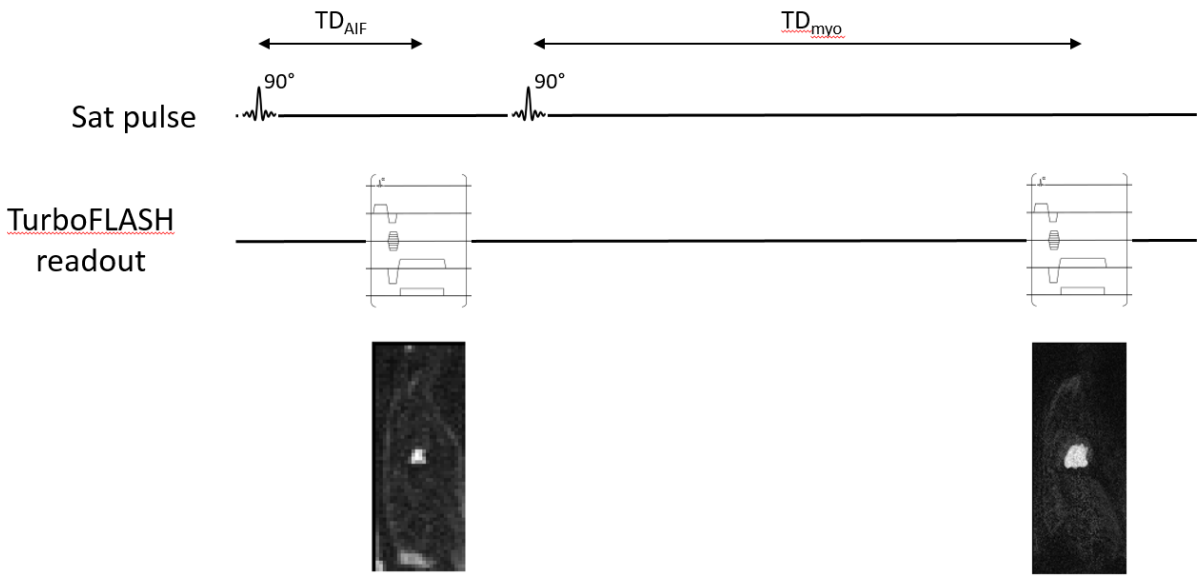

Figure 19: Dual echo pulse sequence
A short TD readout is used to acquire a low res, low SNR, but highly linear image for determining the AIF and a longer TD readout is used to acquire higher SNR myocardial signal

4.3: Methods

4.3.1 Animal Imaging

4 dogs received 3 stress scans each for a total of 12 stress scans. Animal preparation and microsphere quantification were the same as described in Chapter 3. Images were acquired on a 1.5T scanner (Siemens Medical Systems, Erlangen, Germany) with a saturation recovery GRE-EPI acquisition (low TD: TR/TE = 1.33/0.75, flip angle = 8, TD=5, FOV 139.75x344, matrix 26x64; high TD: TR/TE = 1.43/1.52, flip angle = 25, TD=5, FOV 139.75x344, matrix 78x192).

4.3.2 Image Analysis

Image analysis, including contouring, preprocessing, and flow quantification was performed as described in Chapter 3 except for the AIF calculation.

4.3.3 Dual Echo Correction

Both the short TD and long TD AIF data were normalized using the first 10 datapoints. As with the dual bolus correction method, an empiric scaling factor was determined by minimizing the difference between the scaled short TD AIF and the long TD AIF (Figure 20).

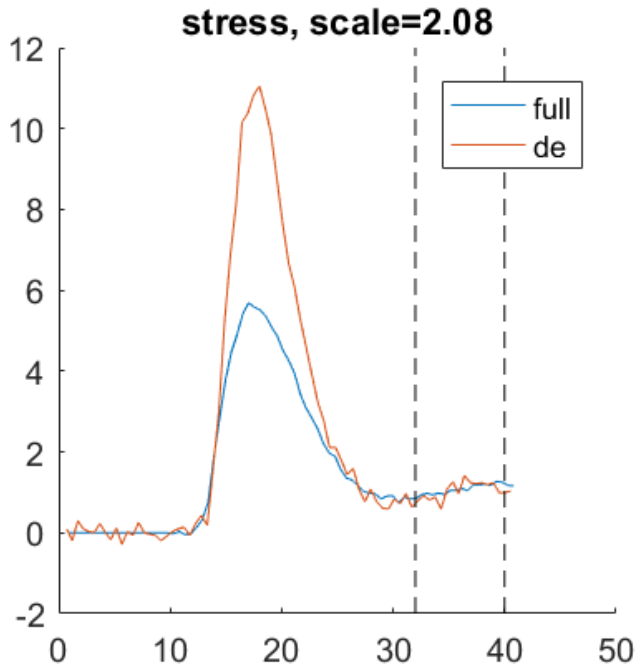

Figure 20: Dual echo tail scaling
Analogous to the method shown in Figure 15, a scaling factor is determined by minimizing differences between the short TD and long TD AIF in the unsaturated region

4.4: Results

The mean scaling factor was 2.02 +/- .39. Correlation plots against microsphere before and after scaling are shown in **Figure 21**. With scaling, the correlation coefficient against microsphere was 0.77 with a best slope of 0.89. Without scaling, 8 sectors had outlier flow values calculated

as greater than 25 mg/ml/min. Even with these outliers removed, the correlation coefficient was 0.72 with a best fit slope of 1.76.

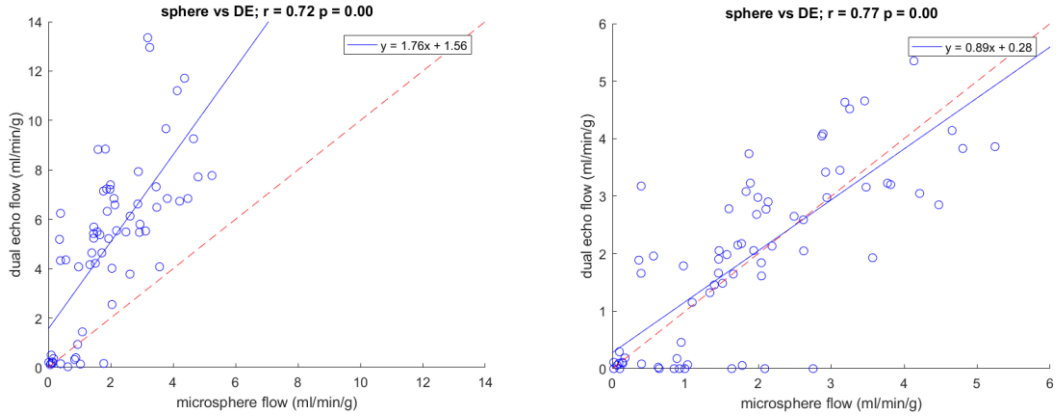

Figure 21: Dual Echo flow vs microsphere
Without any AIF scaling, dual echo dramatically overestimate flow because of the low amplitude of the short TD AIF. With empiric scaling, dual echo flow correlates well with gold-standard microsphere flow

4.5: Discussion

In this study, we evaluated a method for using dual echo sequences to calculate quantitative perfusion values in ml/min/g. While dual echo perfusion *ratios* (MPR) have been shown previously to correlate well with dual bolus perfusion ratios, to our knowledge no study has validated dual echo absolute perfusion values in ml/min/g against a gold-standard measurement. Here, we adapt a technique we developed for dual bolus experiments that uses the unsaturated part of the AIF to appropriately scales the short TD AIF to match the long TD myocardial data. We found this scaling method produced perfusion values that were in excellent agreement with gold-standard microsphere values in an animal model. These results indicate that empiric scaling is a feasible method to use dual echo to obtain quantitative perfusion values in ml/min/g.

Dual echo is a method for quantitative perfusion measurement that has many theoretical advantages. It is currently in the process of being productized, and the prototype sequence is no more difficult to implement than any standard perfusion sequence. Additionally, because the dual echo AIF is sampled from the same first pass bolus as the myocardial data, there is no concern about changing physiological or sequence parameters between scans (as in dual bolus). However, in spite of these advantages, there has been relatively little work using dual echo imaging, and searches on PubMed return roughly equal amount of dual echo and dual bolus perfusion studies.

One impediment to implementing dual echo imaging is knowing how to appropriately scale the short TD AIF. In theory, this could be done by using the scan parameters, baseline PDW images, and the appropriate signal equation. But this can be difficult, changes from scan to scan and sequence to sequence, and can introduce noise. Fortunately the results shown in these experiments show that the empiric AIF scaling method described in Chapter 3 can be readily applied to dual echo data. This method has the advantage of being simple to implement and in theory is broadly applicable to any type of dual sequence imaging. Additionally, we have validated this method against gold-standard microspheres, which to our knowledge has not been done before with dual echo perfusion data.

An important limitation of this work is that we have not yet investigated this method in actual patient data. Currently, all cardiac perfusion MRI scans performed at our institution's hospital use dual echo sequencing, and we are collecting a large amount of dual echo data that can be analyzed. Another limitation is that we have only validated this method in a GRE-EPI sequence, but most clinically acquired perfusion data is acquired using TurboFLASH. The clinical data we

are currently collecting uses a TurboFLASH sequence, so analyzing that data will additionally allow us to investigate whether the method described here is equally applicable in a TurboFLASH sequence. In short, after further validation in a human cohort, this method of implementing dual echo perfusion imaging may represent a simple turn-key solution for acquiring quantitative myocardial perfusion data in a clinical environment.

Chapter 5: Conclusion and Future Directions

Myocardial perfusion is an important marker of cardiovascular health that is routinely used clinically, but paradoxically there has only been limited recent advancement in how myocardial perfusion is measured. SPECT is a technology that is in many ways outclassed by MRI. Compared to MRI, SPECT is lower resolution, involves more radiation, necessitates long wait times by the patient for a stress/rest study (the radioactive isotopes must be cleared from the patient's system before re-imaging), and is incapable of measuring absolute perfusion in ml/min/g. To be fair, SPECT is also lower cost than MRI and (irrespective of patient wait time) can be performed quickly by clinical staff. Still, given the theoretical advantages of MRI in terms of data quality, it is somewhat surprising that myocardial perfusion MRI has not seen greater adoption clinically. In my opinion, a large part of this apparent contradiction is because many of the theoretical advantages of MR perfusion are not easily implemented outside of research environments, and future research into myocardial perfusion MRI would benefit from a more translational approach.

In this dissertation, I discuss one principle advantage that MRI should have: absolute quantification of perfusion in ml/min/g. Intuitively, it seems that measuring a parameter directly should have inherent value, and examination of various clinical scenarios shows that this is fact the case with myocardial perfusion. Relative perfusion values are excellent for identifying focal deficit such as in single vessel coronary artery disease. But the problem with measuring relative perfusion is that it is impossible to distinguish a global deficit from normal perfusion; as long as perfusion is uniformly depressed throughout the myocardium there is no area that stands out relative to the others. So while relative perfusion may easily identify insufficiency in a single

coronary artery, quantitative perfusion has the potential to be of enormous benefit in evaluating multi-vessel disease or any disease that globally affects the microvasculature (e.g. scleroderma or cardiac allograft vasculopathy). Additionally, quantitative values should be superior for monitoring any sort of disease progress over time as quantitative values should have greater scan to scan repeatability than relative values. In short, quantitative perfusion has many immediate theoretical benefits over relative perfusion.

In spite of this theoretical benefit, quantitative perfusion is rarely if ever used in real clinical environments despite many years of research. In 2004, three separate but conceptually similar approaches were published in the literature: dual-bolus, prebolus, and dual echo. All of them, to varying degrees, have been shown to accurately measure quantitative perfusion. Given the obvious benefit of quantitative values and three separate ways shown to quantify perfusion, it is tempting to think that measuring quantitative myocardial perfusion is a solved problem. But over a decade later, there have been scant publications and little use of these techniques outside of a select few large academic centers. In my opinion this is because these techniques as currently implemented, while perfectly acceptable in theory, impose too large a logistical burden in real clinical environments relative to the gains expected from quantitative metrics.

A common thread with published myocardial perfusion techniques is the high degree of technical expertise required. As discussed in Chapters 3 and 4, there are many subtleties to implementing these techniques correctly, and even apparently small mistakes or omissions can lead to large changes in calculated perfusion values. In a research environment, especially in large academic centers with experienced staff, there is enough knowledge, expertise, and time to implement these protocols correctly. But clinical environments are unavoidably more chaotic and time-

restricted. Throughput is important both for timely care and for cost reduction, and widespread adoption would necessarily entail that scans be performed by staff with less expertise than that at large research centers. I believe this explains the apparent disconnect between the status of quantitative perfusion clinically vs in research. The published methods are theoretically and technically sound, but they have not yet easy enough to use to be applied clinically.

This disconnect was the impetus for the work discussed in this dissertation. In Chapter 2, we took the first steps towards implementing a new way to measure myocardial perfusion called the "Bookend" technique. The advantage of this method was not that it would better quantify perfusion relative to dual bolus, prebolus, or dual echo but that it would be easy to use and could be made widely available. This is because Bookend perfusion is something that has already reached easy implementation in the brain. It has been productized, and getting quantitative perfusion is as simple as selecting the appropriate sequence. All of the quantification is done online, and quantitative images are output as part of the sequence's image reconstruction. The goal of the work in Chapter 2 was to take the first steps towards translating this type of ease of use to a cardiac MR environment.

Unfortunately, the contrast agent this technique was predicated on was found to be unsafe. As discussed in Chapter 2, there is good reason to believe that ferumoxytol is safer than the current FDA warning suggests, and it is important to remember that historically there was also significant concern over gadolinium use even though now it is used routinely. While I do think it is appropriate to halt volunteer studies using ferumoxytol, I am optimistic that continued use of ferumoxytol in patient populations will eventually show it to be safe and effective at doses used for contrast imaging. I also believe that myocardial blood volume may be as important a marker

as myocardial perfusion. Once a safe intravascular contrast agent is found and techniques such as those presented in Chapter 2 become more widely available, I believe this will be a very active area of research.

The safety concerns of ferumoxytol caused us to focus more on improving existing quantitative perfusion methods rather than trying to implement in a new one. In doing so, we discovered that there was much that could be done to mitigate some of the logistical difficulty associated with these techniques. In Chapters 3 and 4, we describe a simple yet effective way of scaling arterial signal that not only increases measurement accuracy by removing some physiological noise but also increases tolerance for experimental error. In Chapter 3, when we quantified the difference between assumed vs actual dilution ratios, we found that this experimental error was significant but that it could be retrospectively accounted for and corrected.

If quantification of myocardial perfusion is to become routinely used clinically, it needs to be much easier to implement than it is now. The problem with adoption is not that quantitative perfusion is not good enough, it's that it's not easy enough. This is why I believe that future research should focus less on theoretical improvements to linearity, uniformity, SNR, etc and more on translation to clinical environments. Fortunately, there is currently ongoing research in several areas that would greatly improve the ease of use of quantitative perfusion techniques. This includes work on better motion correction, automatic segmentation, in-line reconstruction, and arrhythmia compensation among other things that all have the potentially to dramatically reduce the logistical complexity of obtaining quantitative perfusion data clinically. I remain optimistic that the research community will succeed is seeing quantitative perfusion successfully

and routinely used in real clinical environments, and I am excited for the new information it will reveal about cardiovascular disease.

References

1. Stirrat, J. and J.A. White, *The prognostic role of late gadolinium enhancement magnetic resonance imaging in patients with cardiomyopathy.* Can J Cardiol, 2013. **29**(3): p. 329-36.
2. Cook, S.C., A.K. Ferketich, and S.V. Raman, *Myocardial ischemia in asymptomatic adults with repaired aortic coarctation.* Int J Cardiol, 2009. **133**(1): p. 95-101.
3. Wang, L., et al., *Coronary risk factors and myocardial perfusion in asymptomatic adults: the Multi-Ethnic Study of Atherosclerosis (MESA).* J Am Coll Cardiol, 2006. **47**(3): p. 565-72.
4. Klocke, F.J., et al., *ACC/AHA/ASNC guidelines for the clinical use of cardiac radionuclide imaging--executive summary: a report of the American College of Cardiology/American Heart Association Task Force on Practice Guidelines (ACC/AHA/ASNC Committee to Revise the 1995 Guidelines for the Clinical Use of Cardiac Radionuclide Imaging).* J Am Coll Cardiol, 2003. **42**(7): p. 1318-33.
5. Jerosch-Herold, M., *Quantification of myocardial perfusion by cardiovascular magnetic resonance.* J Cardiovasc Magn Reson, 2010. **12**: p. 57.
6. Kellman, P. and A.E. Arai, *Imaging sequences for first pass perfusion --a review.* J Cardiovasc Magn Reson, 2007. **9**(3): p. 525-37.
7. Coelho-Filho, O.R., et al., *MR myocardial perfusion imaging.* Radiology, 2013. **266**(3): p. 701-15.
8. Gerber, B.L., et al., *Myocardial first-pass perfusion cardiovascular magnetic resonance: history, theory, and current state of the art.* J Cardiovasc Magn Reson, 2008. **10**: p. 18.
9. Jerosch-Herold, M., et al., *Analysis of myocardial perfusion MRI.* J Magn Reson Imaging, 2004. **19**(6): p. 758-70.
10. Zhang, H., et al., *Accurate myocardial T1 measurements: toward quantification of myocardial blood flow with arterial spin labeling.* Magn Reson Med, 2005. **53**(5): p. 1135-42.
11. Wright, K.B., et al., *Assessment of regional differences in myocardial blood flow using T2-weighted 3D BOLD imaging.* Magn Reson Med, 2001. **46**(3): p. 573-8.
12. Lee, D.C.C., N. R.; Carroll, T.J., in *Basic Principles of Cardiovascular MRI*, M.A.R. Syed, S. V; Simonetti, O.P., Editor. 2016, Springer. p. 179-192.
13. Tsekos, N.V., et al., *Fast anatomical imaging of the heart and assessment of myocardial perfusion with arrhythmia insensitive magnetization preparation.* Magn Reson Med, 1995. **34**(4): p. 530-6.
14. Kim, D., A. Cernicanu, and L. Axel, *B(0) and B(1)-insensitive uniform T(1)-weighting for quantitative, first-pass myocardial perfusion magnetic resonance imaging.* Magn Reson Med, 2005. **54**(6): p. 1423-9.
15. Kim, D., et al., *Comparison of the effectiveness of saturation pulses in the heart at 3T.* Magn Reson Med, 2008. **59**(1): p. 209-15.
16. Haase, A., et al., *Inversion recovery snapshot FLASH MR imaging.* J Comput Assist Tomogr, 1989. **13**(6): p. 1036-40.
17. Ding, S., S.D. Wolff, and F.H. Epstein, *Improved coverage in dynamic contrast-enhanced cardiac MRI using interleaved gradient-echo EPI.* Magn Reson Med, 1998. **39**(4): p. 514-9.

18. Schreiber, W.G., et al., *Dynamic contrast-enhanced myocardial perfusion imaging using saturation-prepared TrueFISP.* J Magn Reson Imaging, 2002. **16**(6): p. 641-52.
19. Fenchel, M., et al., *Multislice first-pass myocardial perfusion imaging: Comparison of saturation recovery (SR)-TrueFISP-two-dimensional (2D) and SR-TurboFLASH-2D pulse sequences.* J Magn Reson Imaging, 2004. **19**(5): p. 555-63.
20. Lyne, J.C., et al., *Direct comparison of myocardial perfusion cardiovascular magnetic resonance sequences with parallel acquisition.* J Magn Reson Imaging, 2007. **26**(6): p. 1444-51.
21. Sodickson, D.K. and W.J. Manning, *Simultaneous acquisition of spatial harmonics (SMASH): fast imaging with radiofrequency coil arrays.* Magn Reson Med, 1997. **38**(4): p. 591-603.
22. Pruessmann, K.P., et al., *SENSE: sensitivity encoding for fast MRI.* Magn Reson Med, 1999. **42**(5): p. 952-62.
23. Griswold, M.A., et al., *Generalized autocalibrating partially parallel acquisitions (GRAPPA).* Magn Reson Med, 2002. **47**(6): p. 1202-10.
24. Tsao, J., P. Boesiger, and K.P. Pruessmann, *k-t BLAST and k-t SENSE: dynamic MRI with high frame rate exploiting spatiotemporal correlations.* Magn Reson Med, 2003. **50**(5): p. 1031-42.
25. Mistretta, C.A., et al., *Highly constrained backprojection for time-resolved MRI.* Magn Reson Med, 2006. **55**(1): p. 30-40.
26. Ge, L., et al., *Myocardial perfusion MRI with sliding-window conjugate-gradient HYPR.* Magn Reson Med, 2009. **62**(4): p. 835-9.
27. Kozerke, S. and J. Tsao, *Reduced data acquisition methods in cardiac imaging.* Top Magn Reson Imaging, 2004. **15**(3): p. 161-8.
28. Grist, T.M., et al., *Time-resolved angiography: Past, present, and future.* J Magn Reson Imaging, 2012. **36**(6): p. 1273-86.
29. Deshmane, A., et al., *Parallel MR imaging.* J Magn Reson Imaging, 2012. **36**(1): p. 55-72.
30. Pedersen, H., et al., *Quantification of myocardial perfusion using free-breathing MRI and prospective slice tracking.* Magn Reson Med, 2009. **61**(3): p. 734-8.
31. Milles, J., et al., *Fully automated motion correction in first-pass myocardial perfusion MR image sequences.* IEEE Trans Med Imaging, 2008. **27**(11): p. 1611-21.
32. Stegmann, M.B., H. Olafsdottir, and H.B. Larsson, *Unsupervised motion-compensation of multi-slice cardiac perfusion MRI.* Med Image Anal, 2005. **9**(4): p. 394-410.
33. Bidaut, L.M. and J.P. Vallee, *Automated registration of dynamic MR images for the quantification of myocardial perfusion.* J Magn Reson Imaging, 2001. **13**(4): p. 648-55.
34. Yang, G.Z., et al., *Motion and deformation tracking for short-axis echo-planar myocardial perfusion imaging.* Med Image Anal, 1998. **2**(3): p. 285-302.
35. Scott, A.D., J. Keegan, and D.N. Firmin, *Motion in cardiovascular MR imaging.* Radiology, 2009. **250**(2): p. 331-51.
36. Di Bella, E.V., D.L. Parker, and A.J. Sinusas, *On the dark rim artifact in dynamic contrast-enhanced MRI myocardial perfusion studies.* Magn Reson Med, 2005. **54**(5): p. 1295-9.
37. Sharma, P., et al., *Effect of Gd-DTPA-BMA on blood and myocardial T1 at 1.5T and 3T in humans.* J Magn Reson Imaging, 2006. **23**(3): p. 323-30.

38. Kim, D. and L. Axel, *Multislice, dual-imaging sequence for increasing the dynamic range of the contrast-enhanced blood signal and CNR of myocardial enhancement at 3T.* J Magn Reson Imaging, 2006. **23**(1): p. 81-6.
39. Noeske, R., et al., *Human cardiac imaging at 3 T using phased array coils.* Magn Reson Med, 2000. **44**(6): p. 978-82.
40. Klem, I., et al., *Improved detection of coronary artery disease by stress perfusion cardiovascular magnetic resonance with the use of delayed enhancement infarction imaging.* J Am Coll Cardiol, 2006. **47**(8): p. 1630-8.
41. Tofts, P.S., et al., *Estimating kinetic parameters from dynamic contrast-enhanced T(1)-weighted MRI of a diffusable tracer: standardized quantities and symbols.* J Magn Reson Imaging, 1999. **10**(3): p. 223-32.
42. Ishida, M., et al., *Quantification of myocardial blood flow using model based analysis of first-pass perfusion MRI: extraction fraction of Gd-DTPA varies with myocardial blood flow in human myocardium.* Magn Reson Med, 2011. **66**(5): p. 1391-9.
43. Thompson, H.K., Jr., et al., *Indicator Transit Time Considered as a Gamma Variate.* Circ Res, 1964. **14**: p. 502-15.
44. Christian, T.F., et al., *Absolute myocardial perfusion in canines measured by using dual-bolus first-pass MR imaging.* Radiology, 2004. **232**(3): p. 677-84.
45. Kostler, H., et al., *Prebolus quantitative MR heart perfusion imaging.* Magn Reson Med, 2004. **52**(2): p. 296-9.
46. Gatehouse, P.D., et al., *Accurate assessment of the arterial input function during high-dose myocardial perfusion cardiovascular magnetic resonance.* J Magn Reson Imaging, 2004. **20**(1): p. 39-45.
47. Sakaie, K.E., et al., *Method for improving the accuracy of quantitative cerebral perfusion imaging.* J Magn Reson Imaging, 2005. **21**(5): p. 512-9.
48. Parikh V, L.J., Shin W, Mouannes J, Videen T, Snyder A, Derdeyn C, Carroll T. *qCBF: A Comparison of the Accuracy Between the Bookend Technique, Empirical Reference Values and [O15]-H20 PET in*

Moyamoya Patients. in *International Society of Magnetic Resonance in Medicine 17th Scientific Meeting and Exhibition*. 2009. Honolulu, Hawai'i, USA.
49. Shin, W., et al., *Quantitative cerebral perfusion using dynamic susceptibility contrast MRI: evaluation of reproducibility and age- and gender-dependence with fully automatic image postprocessing algorithm.* Magn Reson Med, 2007. **58**(6): p. 1232-41.
50. Shah, M.K., et al., *Method for rapid calculation of quantitative cerebral perfusion.* J Magn Reson Imaging, 2008. **28**(5): p. 1258-65.
51. Sakaie, K.E., W. Shin, and T.J. Carroll. *Comparison Of Analysis Methods for T1 Measurement by trueFISP Readout of Inversion Recovery*. in *ISMRM 12th Scientific Meeting and Exhibition*. 2004.
52. Salisbury, P.F., C.E. Cross, and P.A. Rieben, *Physiological factors influencing coronary blood volume in isolated dog hearts.* Am J Physiol, 1961. **200**: p. 633-6.
53. Rakusan, K., *Quantitative morphology of capillaries of the heart. Number of capillaries in animal and human hearts under normal and pathological conditions.* Methods Achiev Exp Pathol, 1971. **5**: p. 272-86.

54. Le, D.E., et al., *Changes in myocardial blood volume over a wide range of coronary driving pressures: role of capillaries beyond the autoregulatory range.* Heart, 2004. **90**(10): p. 1199-205.
55. Rutz, T., et al., *Quantitative myocardial contrast echocardiography: a new method for the non-invasive detection of chronic heart transplant rejection.* Eur Heart J Cardiovasc Imaging, 2013. **14**(12): p. 1187-94.
56. McCommis, K.S., et al., *Roles of myocardial blood volume and flow in coronary artery disease: an experimental MRI study at rest and during hyperemia.* Eur Radiol, 2010. **20**(8): p. 2005-12.
57. Mohlenkamp, S., et al., *Coronary microvascular functional reserve: quantification of long-term changes with electron-beam CT preliminary results in a porcine model.* Radiology, 2001. **221**(1): p. 229-36.
58. Waller, C., et al., *Myocardial perfusion and intracapillary blood volume in rats at rest and with coronary dilatation: MR imaging in vivo with use of a spin-labeling technique.* Radiology, 2000. **215**(1): p. 189-97.
59. Captur, G., C. Manisty, and J.C. Moon, *Cardiac MRI evaluation of myocardial disease.* Heart, 2016.
60. Donahue, K.M., et al., *Improving MR quantification of regional blood volume with intravascular T1 contrast agents: accuracy, precision, and water exchange.* Magn Reson Med, 1996. **36**(6): p. 858-67.
61. Hazlewood, C.F., et al., *Nuclear magnetic resonance transverse relaxation times of water protons in skeletal muscle.* Biophys J, 1974. **14**(8): p. 583-606.
62. Bane, O., et al., *Leakage and water exchange characterization of gadofosveset in the myocardium.* Magn Reson Imaging, 2014. **32**(3): p. 224-35.
63. Port, M., et al., *How to compare the efficiency of albumin-bound and nonalbumin-bound contrast agents in vivo: the concept of dynamic relaxivity.* Invest Radiol, 2005. **40**(9): p. 565-73.
64. Li, W., et al., *First-pass contrast-enhanced magnetic resonance angiography in humans using ferumoxytol, a novel ultrasmall superparamagnetic iron oxide (USPIO)-based blood pool agent.* J Magn Reson Imaging, 2005. **21**(1): p. 46-52.
65. Stabi, K.L. and L.M. Bendz, *Ferumoxytol use as an intravenous contrast agent for magnetic resonance angiography.* Ann Pharmacother, 2011. **45**(12): p. 1571-5.
66. Varallyay, C.G., et al., *High-resolution steady-state cerebral blood volume maps in patients with central nervous system neoplasms using ferumoxytol, a superparamagnetic iron oxide nanoparticle.* J Cereb Blood Flow Metab, 2013.
67. Marty, B., et al., *BLOCH equations-based reconstruction of myocardium t1 maps from modified look-locker inversion recovery sequence.* PLoS One, 2015. **10**(5): p. e0126766.
68. Hamilton, B.E., et al., *Comparative analysis of ferumoxytol and gadoteridol enhancement using T1- and T2-weighted MRI in neuroimaging.* AJR Am J Roentgenol, 2011. **197**(4): p. 981-8.
69. *FDA Drug Safety Communication: FDA strengthens warnings and changes prescribing instructions to decrease the risk of serious allergic reactions with anemia drug Feraheme (ferumoxytol).* 2015, FDA.
70. Vasanawala, S.S., et al., *Safety and technique of ferumoxytol administration for MRI.* Magn Reson Med, 2016. **75**(5): p. 2107-11.

71. Finn, J.P., et al., *Cardiovascular MRI with ferumoxytol.* Clin Radiol, 2016. **71**(8): p. 796-806.
72. Ishida, M., et al., *Development of a universal dual-bolus injection scheme for the quantitative assessment of myocardial perfusion cardiovascular magnetic resonance.* J Cardiovasc Magn Reson, 2011. **13**: p. 28.
73. Keijer, J.T., et al., *Semiquantitation of regional myocardial blood flow in normal human subjects by first-pass magnetic resonance imaging.* Am Heart J, 1995. **130**(4): p. 893-901.
74. Shen, Y., et al., *T1 relaxivities of gadolinium-based magnetic resonance contrast agents in human whole blood at 1.5, 3, and 7 T.* Invest Radiol, 2015. **50**(5): p. 330-8.
75. Lee, D.C., et al., *Magnetic resonance versus radionuclide pharmacological stress perfusion imaging for flow-limiting stenoses of varying severity.* Circulation, 2004. **110**(1): p. 58-65.
76. Cerqueira, M.D., et al., *Standardized myocardial segmentation and nomenclature for tomographic imaging of the heart. A statement for healthcare professionals from the Cardiac Imaging Committee of the Council on Clinical Cardiology of the American Heart Association.* Circulation, 2002. **105**(4): p. 539-42.
77. Glenny, R.W., S. Bernard, and M. Brinkley, *Validation of fluorescent-labeled microspheres for measurement of regional organ perfusion.* J Appl Physiol (1985), 1993. **74**(5): p. 2585-97.
78. Pack, N.A. and E.V. DiBella, *Comparison of myocardial perfusion estimates from dynamic contrast-enhanced magnetic resonance imaging with four quantitative analysis methods.* Magn Reson Med, 2010. **64**(1): p. 125-37.
79. Zou, G.Y., *Toward using confidence intervals to compare correlations.* Psychol Methods, 2007. **12**(4): p. 399-413.
80. Baguley, T. *Comparing correlations: independent and dependent (overlapping or non-overlapping).* 2012; Available from: https://seriousstats.wordpress.com/2012/02/05/comparing-correlations/.
81. Groothuis, J.G., et al., *Comparison of dual to single contrast bolus magnetic resonance myocardial perfusion imaging for detection of significant coronary artery disease.* J Magn Reson Imaging, 2010. **32**(1): p. 88-93.
82. Utz, W., et al., *Single- or dual-bolus approach for the assessment of myocardial perfusion reserve in quantitative MR perfusion imaging.* Magn Reson Med, 2008. **59**(6): p. 1373-7.
83. Fluckiger, J.U., M.C. Schabel, and E.V. DiBella, *Constrained estimation of the arterial input function for myocardial perfusion cardiovascular magnetic resonance.* Magn Reson Med, 2011. **66**(2): p. 419-27.